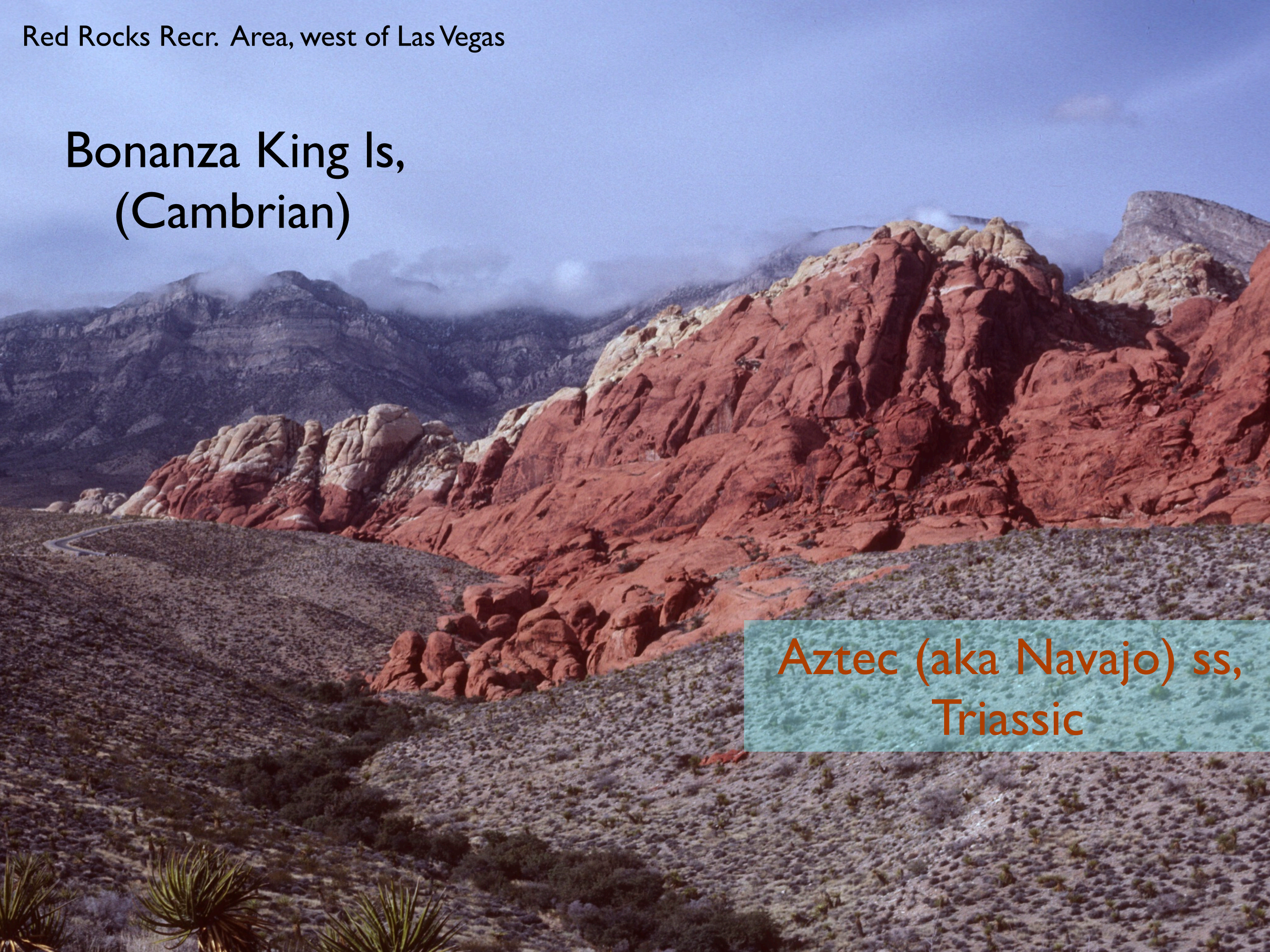
Red Rocks Recr. Area, west of Las Vegas
Bonanza King ls,
(Cambrian)
Aztec (aka Navajo) ss,
Triassic


88 4 1

Eastern Spring Mountains

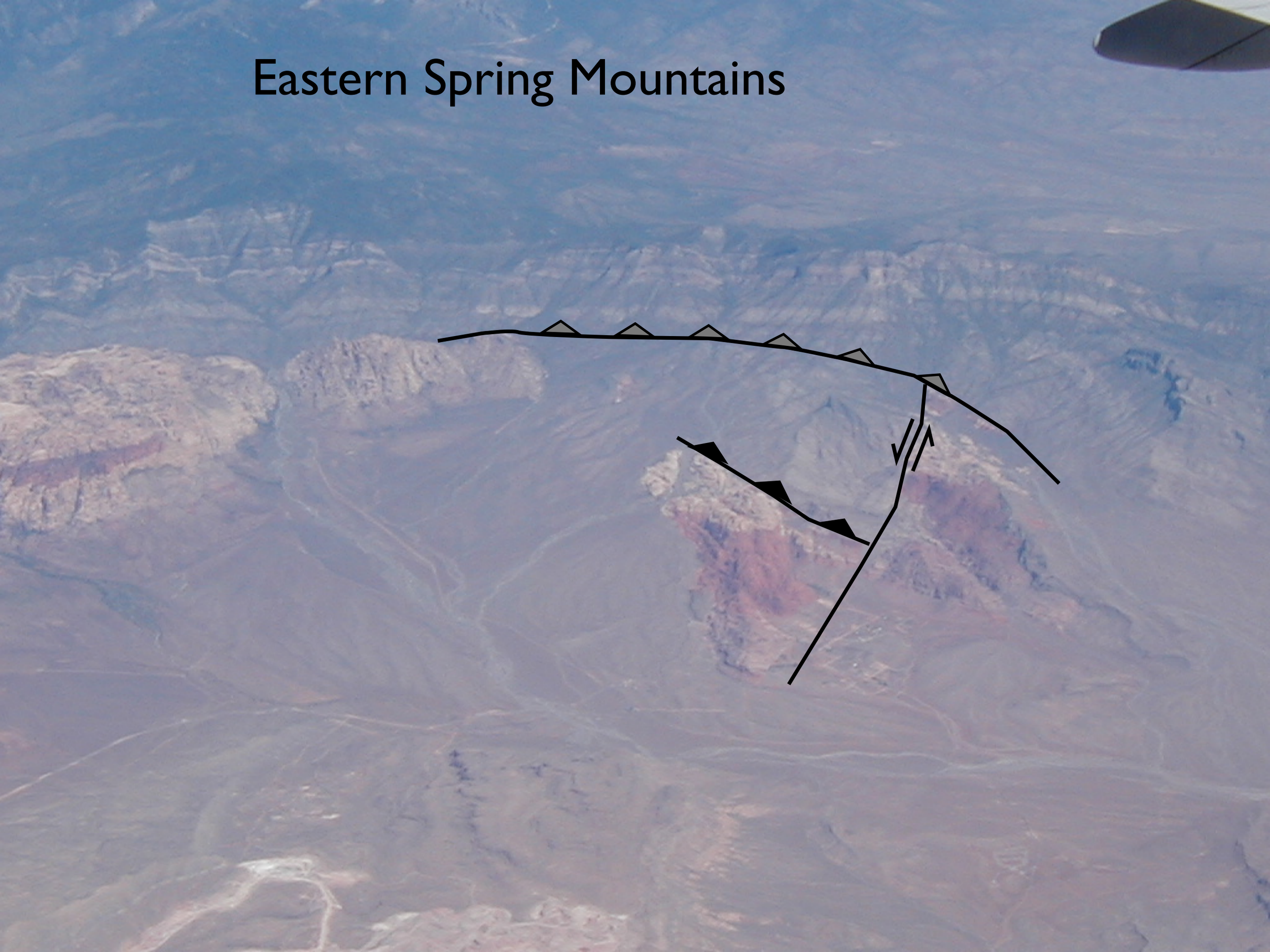

Muddy Mountains Thrust


Overton conglomerate

Luning-Fencemaker thrust belt mid or late J to K

Central Nevada thrust belt (Ely belt) mid-J to Cretaceous

Sevier thrust belt late J to early T

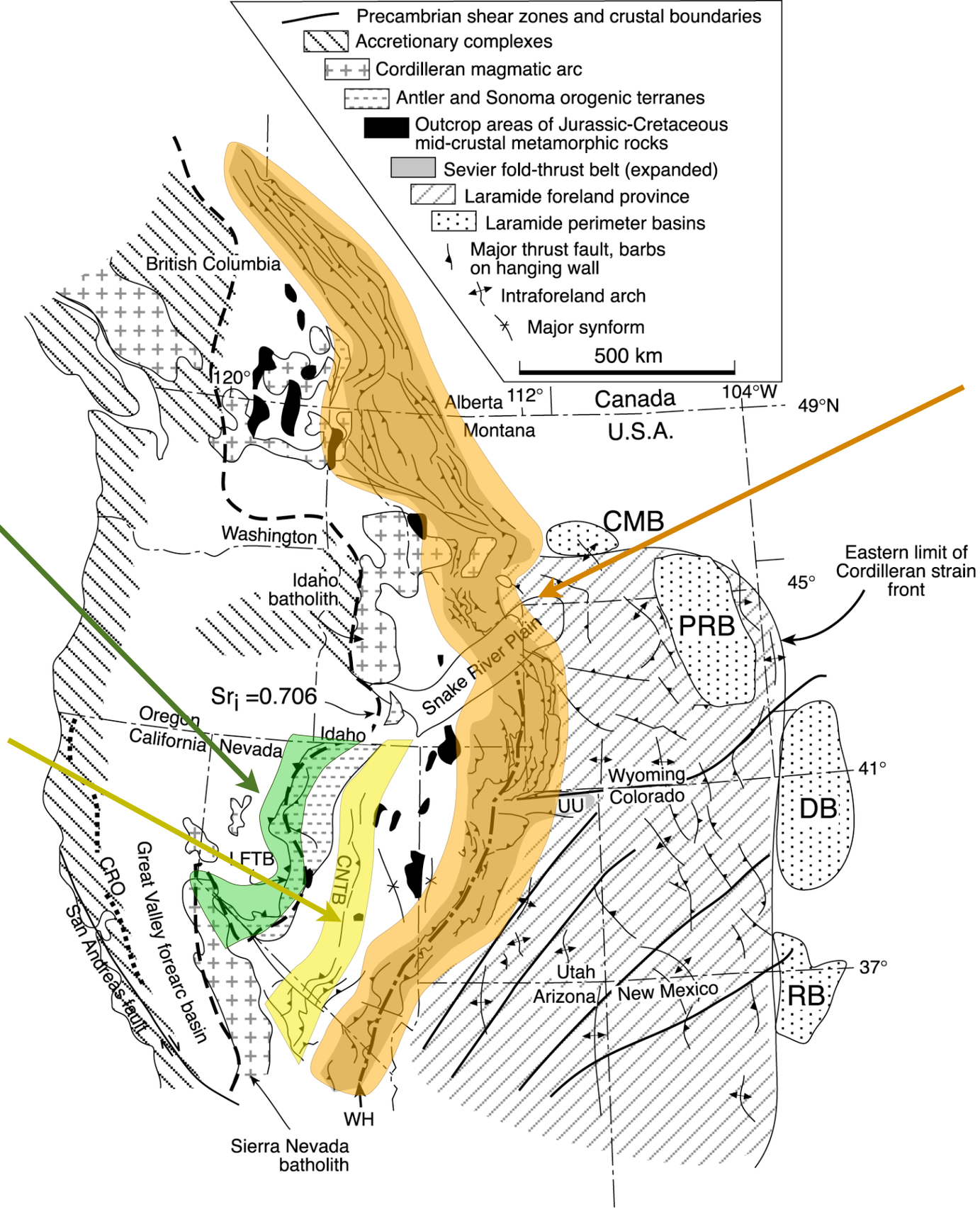

Fig. 2. Tectonic map of the western United States, showing the major components of the Cordilleran orogenic belt. The initial Sr ratio line is taken to represent the approximate western edge of North American cratonic basement (Armstrong and others, 1977; Kistler and Peterman, 1978). Abbreviations as follows: CRO, Coast Range ophiolite; LFTB, Luning-Fencemaker thrust belt; CNTB, Central Nevada thrust belt; WH, Wasatch hinge line; UU, Uinta Mountains uplift; CMB, Crazy Mountains basin; PRB, Powder River basin; DB, Denver basin; RB, Raton basin. Precambrian shear zones after Karlstrom and Williams (1998).

DeCelles, *Am J Sci*, 2004

Convergent margin terminology

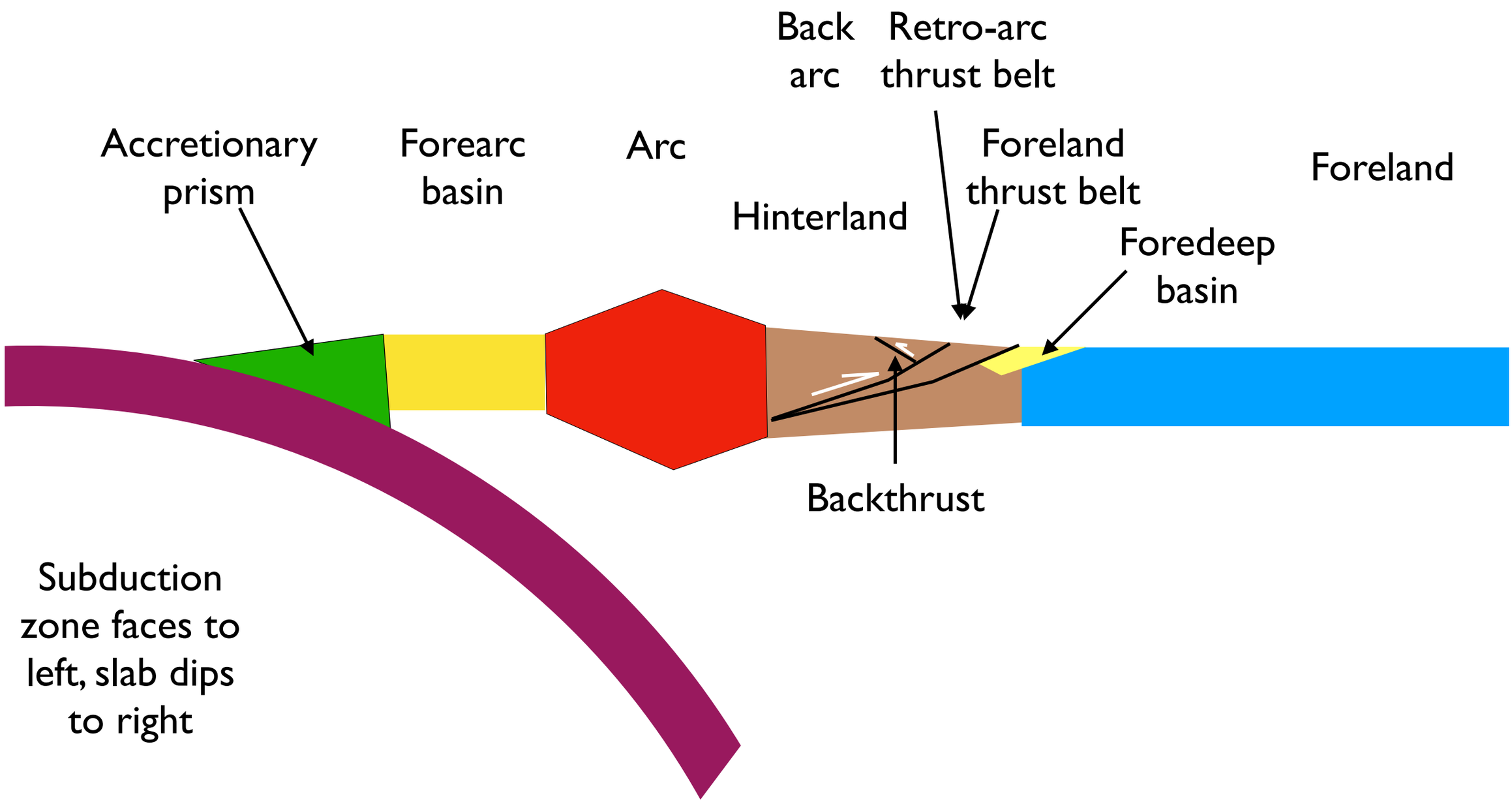

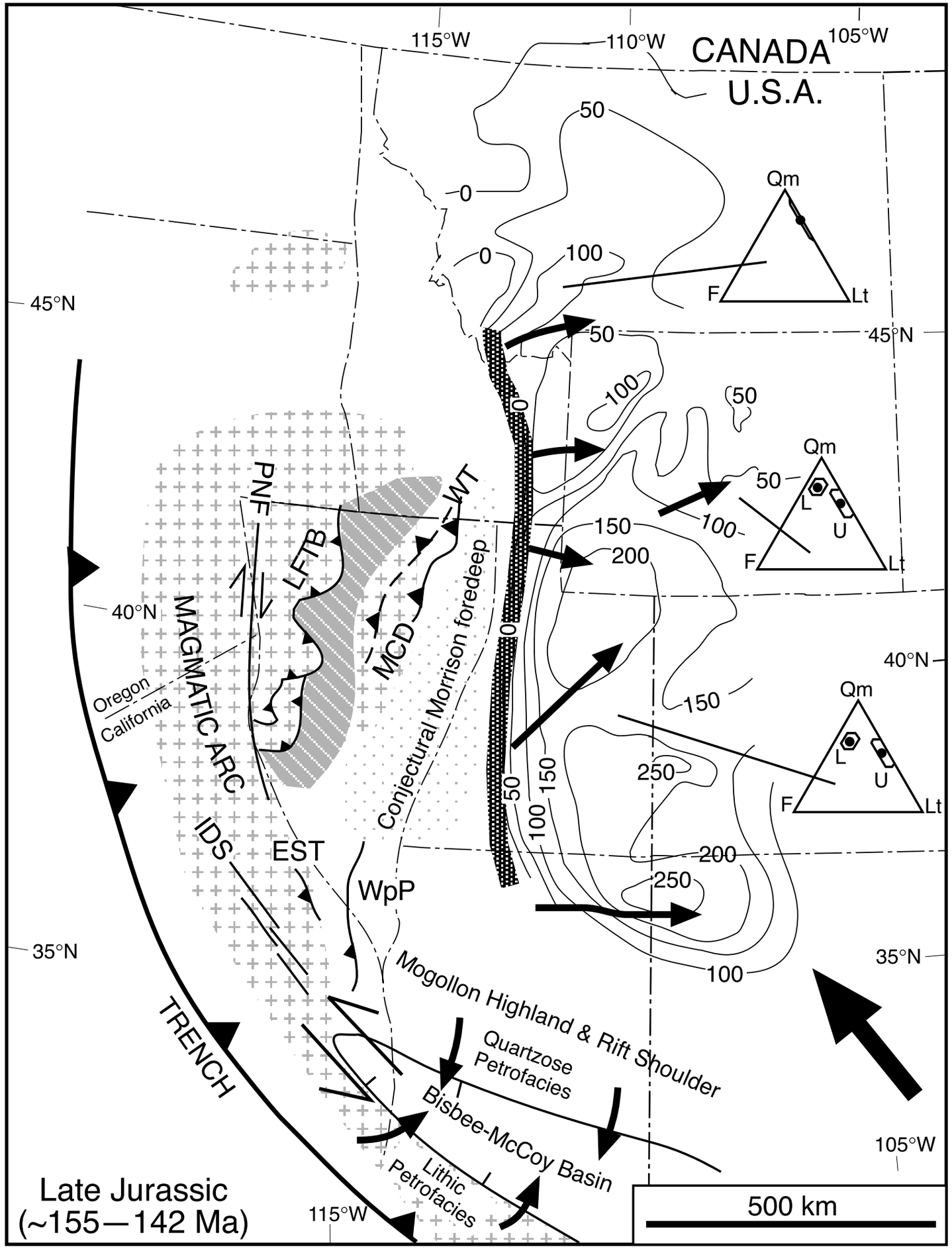

DeCelles, *Am J Sci*, 2004

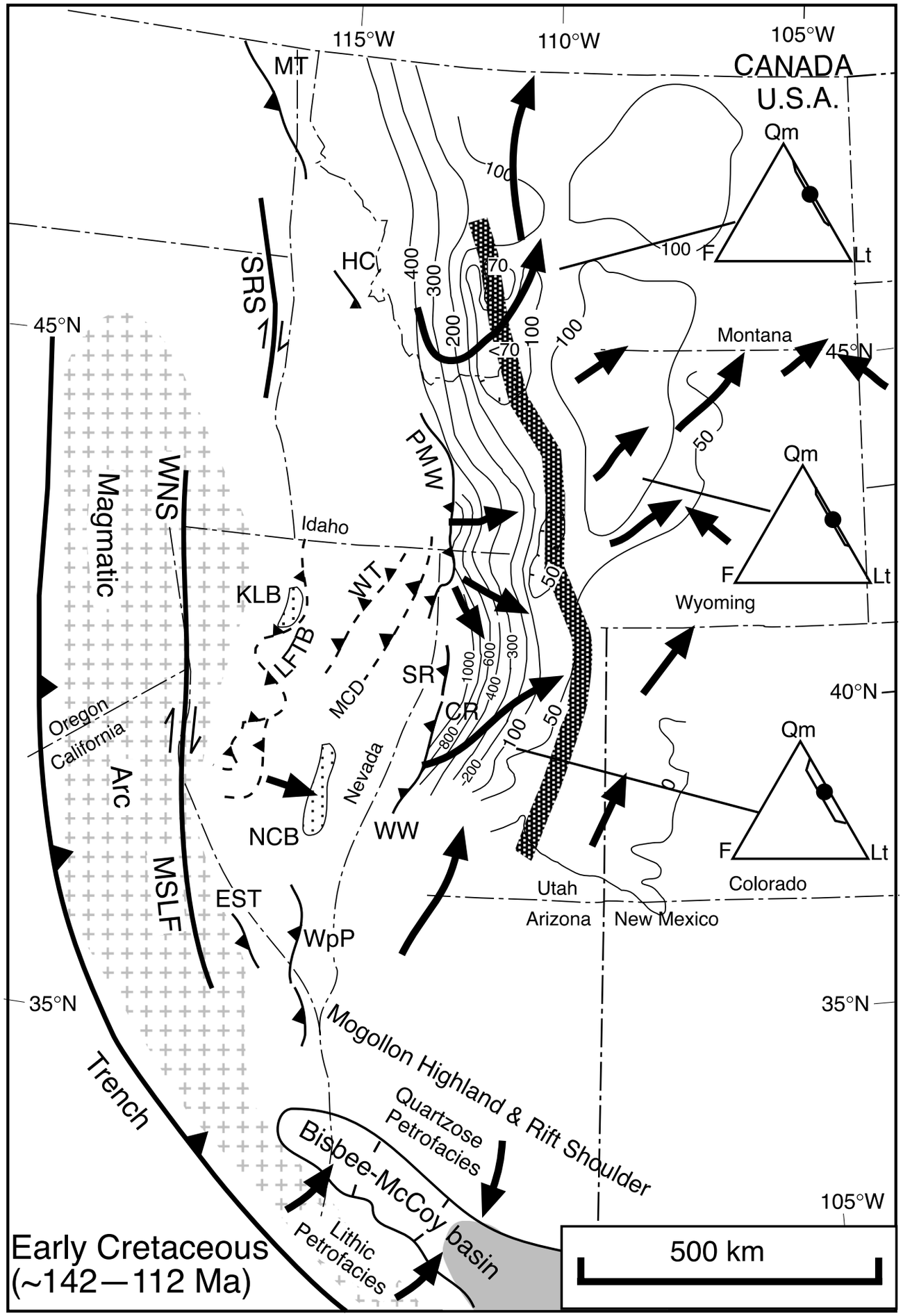

DeCelles, *Am J Sci*, 2004

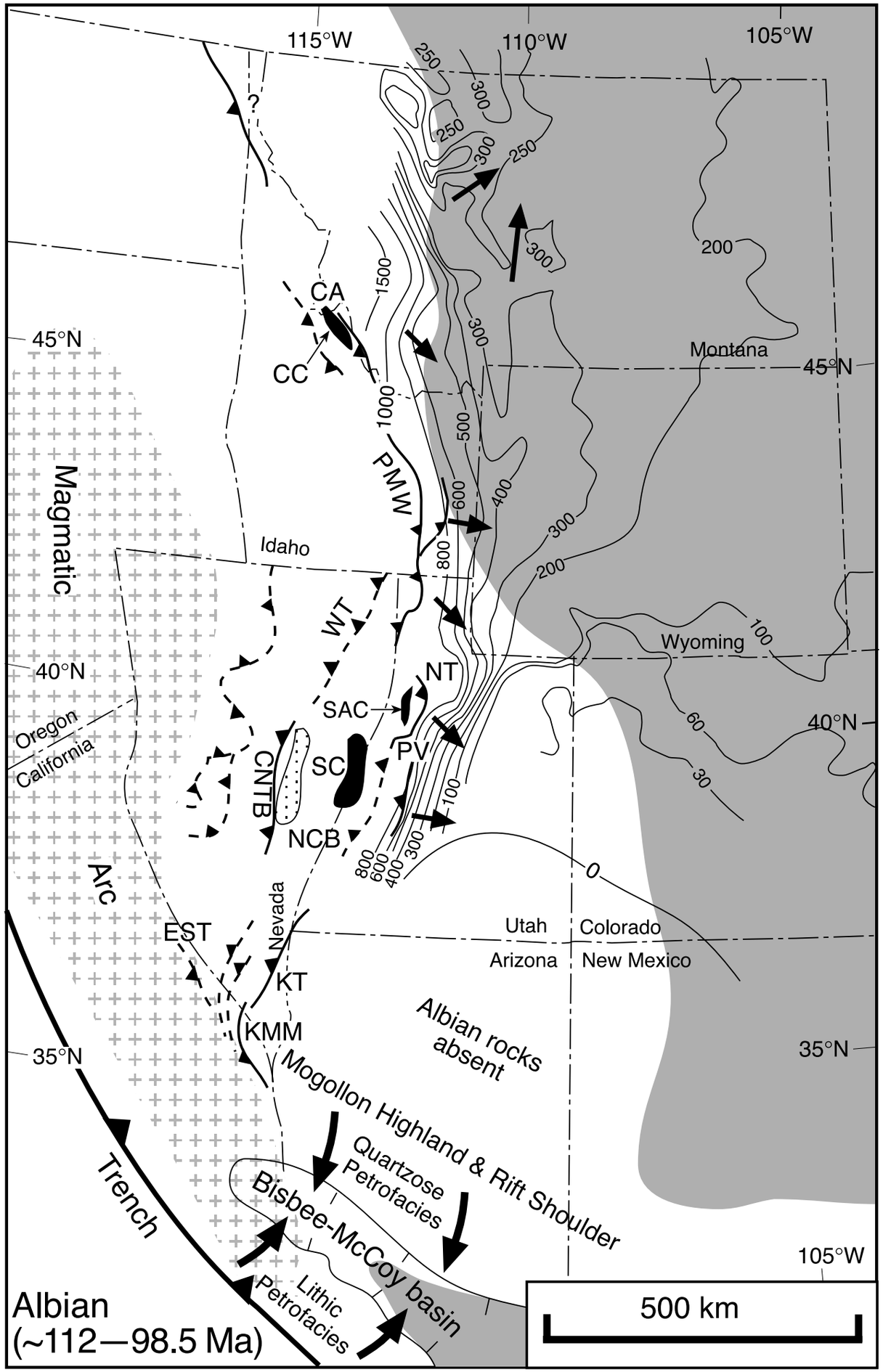

DeCelles, *Am J Sci*, 2004

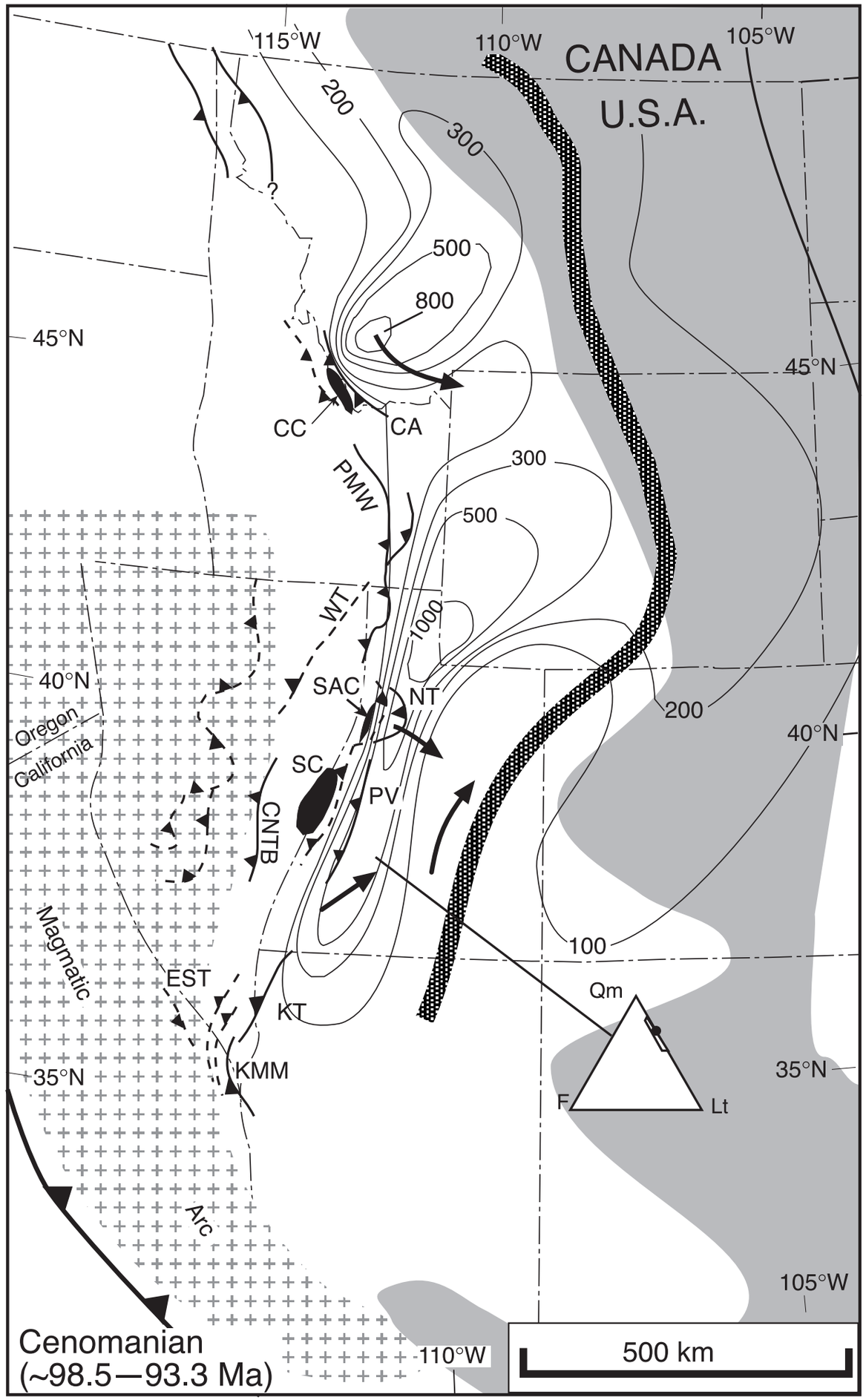

DeCelles, *Am J Sci*, 2004

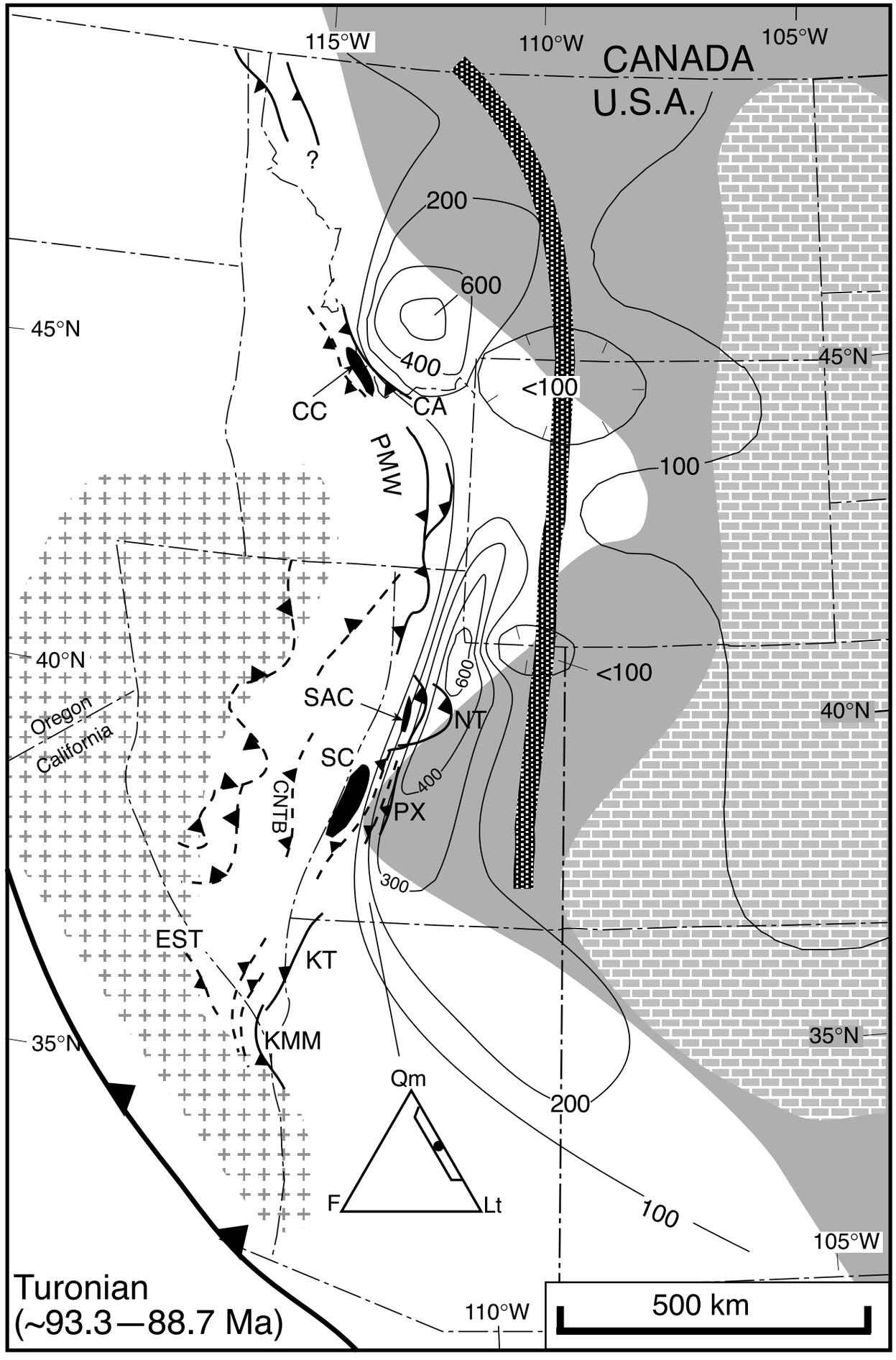

DeCelles, *Am J Sci*, 2004

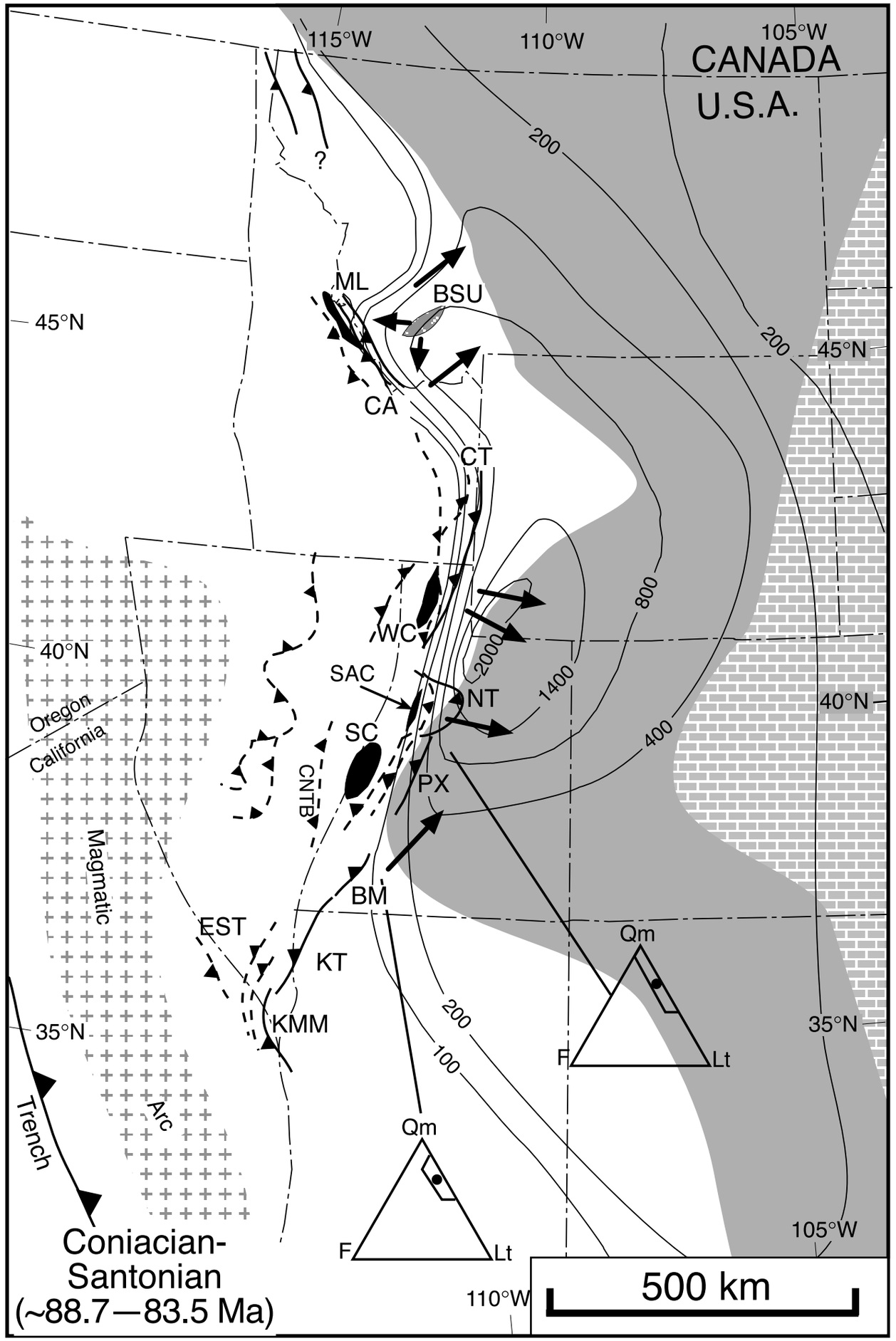

DeCelles, *Am J Sci*, 2004

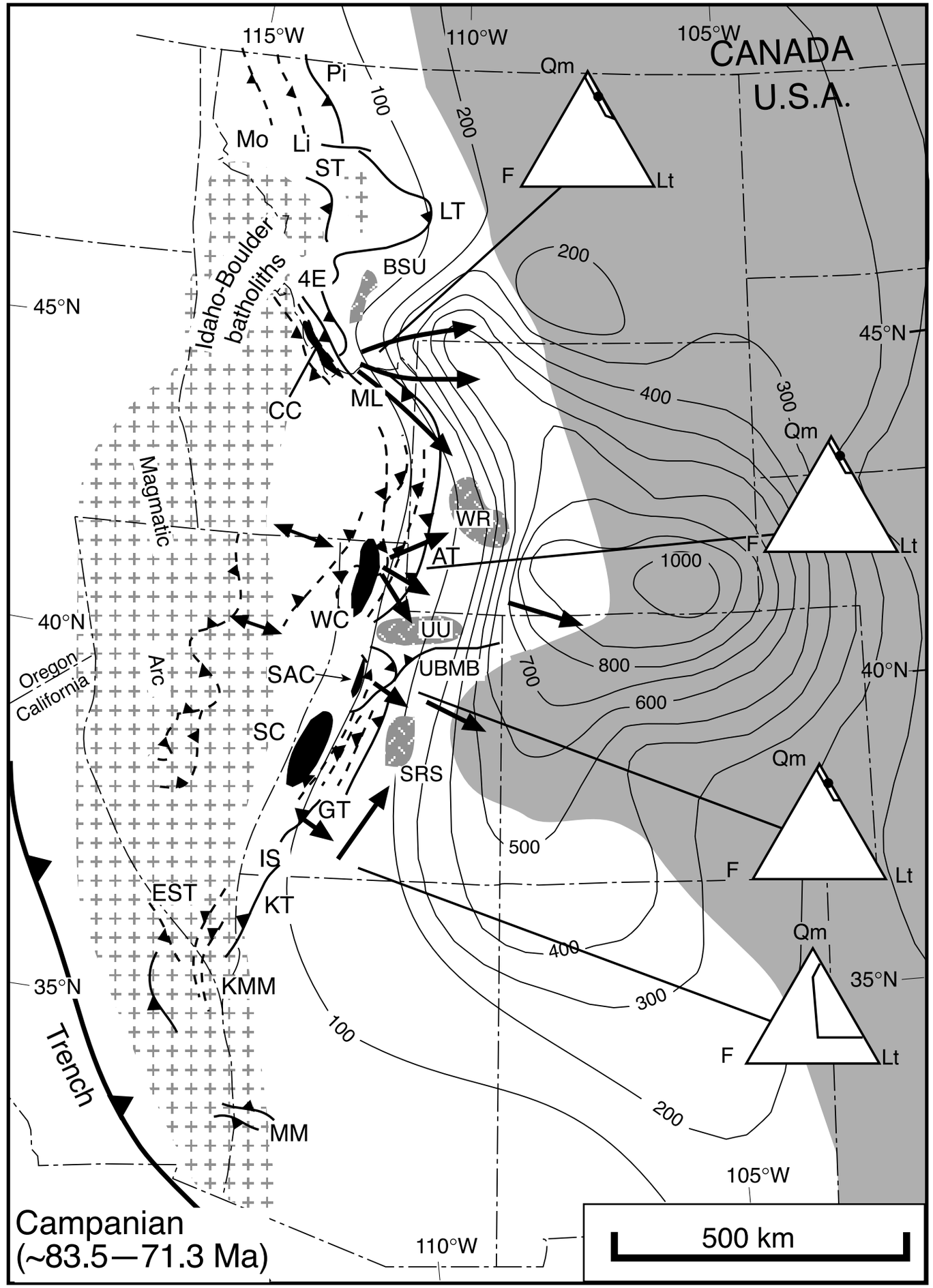

Note: Isopachs here were displaced to the east several hundred kilometers in a drafting mistake

DeCelles, *Am J Sci*, 2004

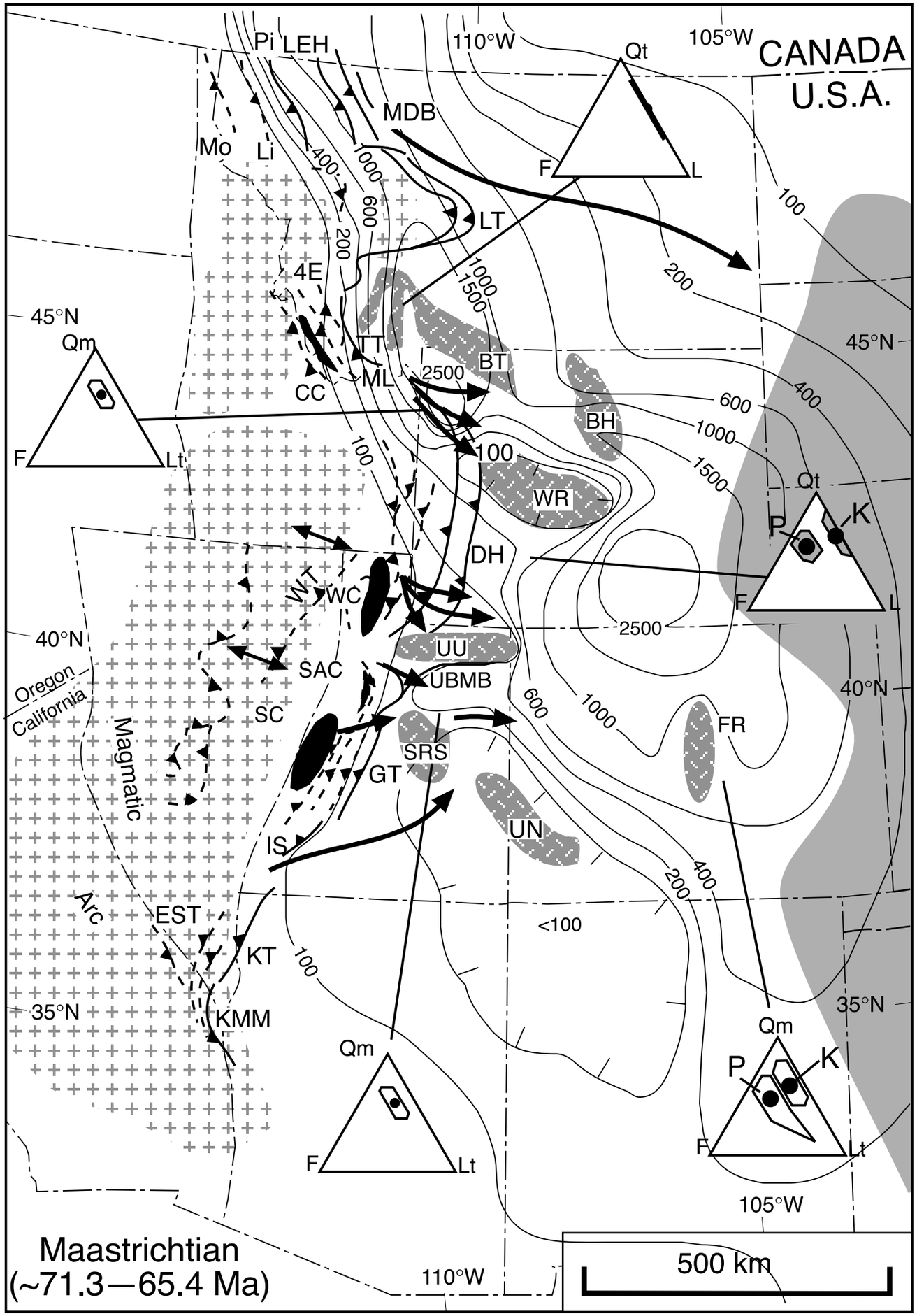

DeCelles, *Am J Sci*, 2004

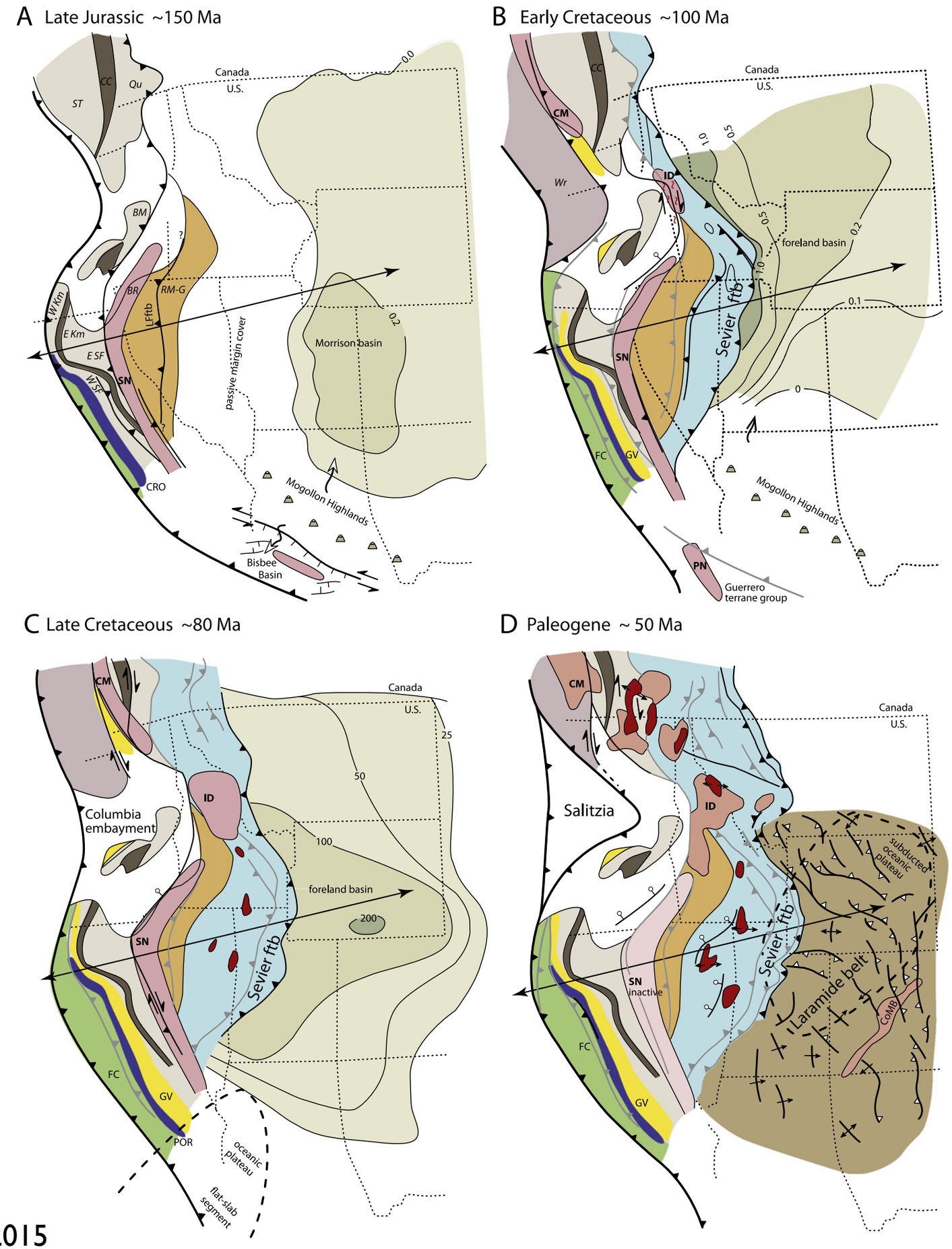

Yonkee & Weil, *Earth Sci Rev*, 2015

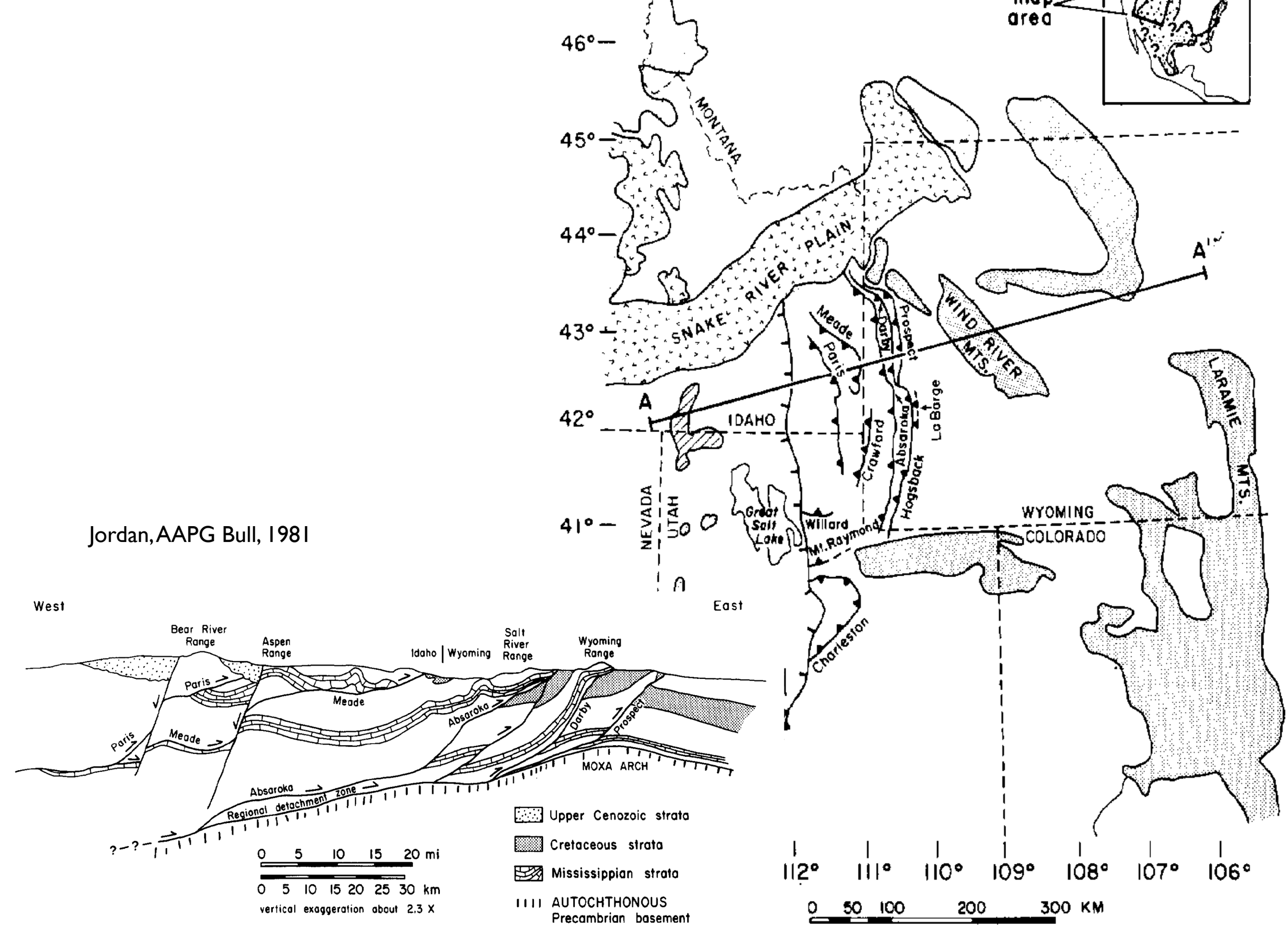

FIG. 2—Generalized schematic cross section across Idaho-Wyoming thrust belt along line AA′ of Figure 1 (after cross section XX′ of Royse et al, 1975), illustrating west-dipping sledrunner form of thrust faults and duplication of section.

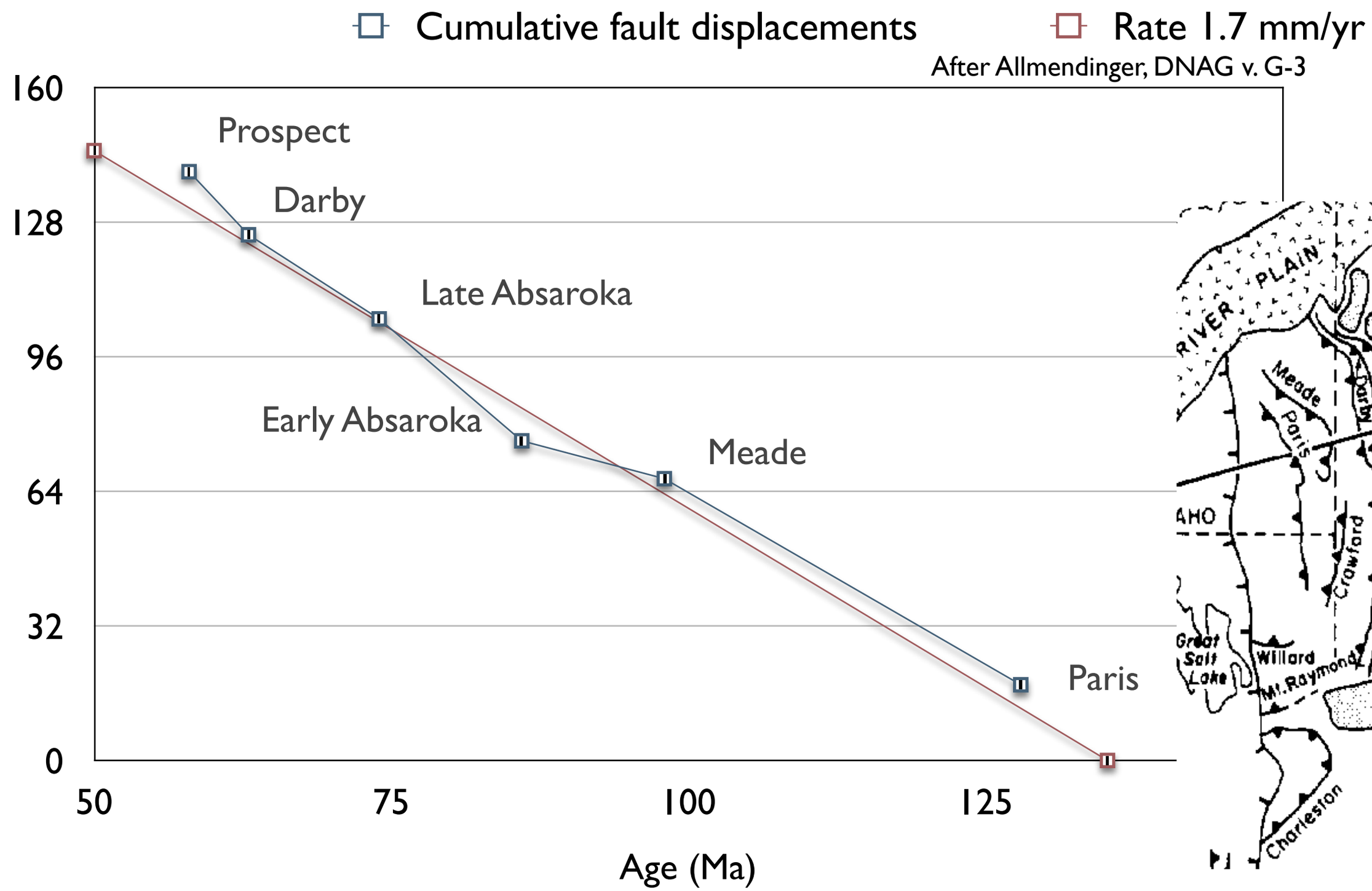

When thrusts get younger in the foreland direction, they are considered to be *in sequence*. If a thrust towards the hinterland is younger, it is *out of sequence*.

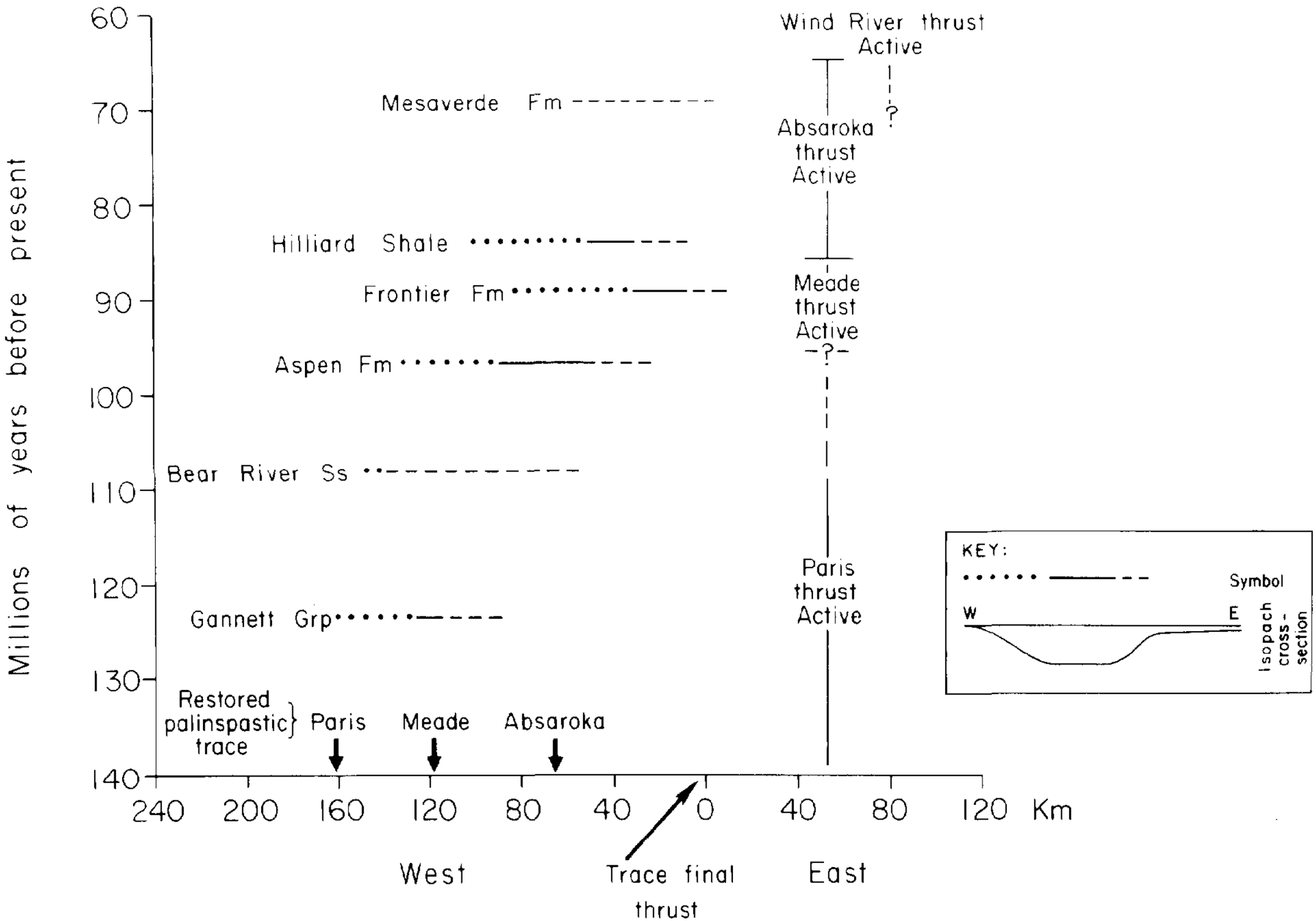

FIG. 12—Graph showing eastward shift of palinspastic position of foreland trough through time.

Jordan, AAPG Bull, 1981

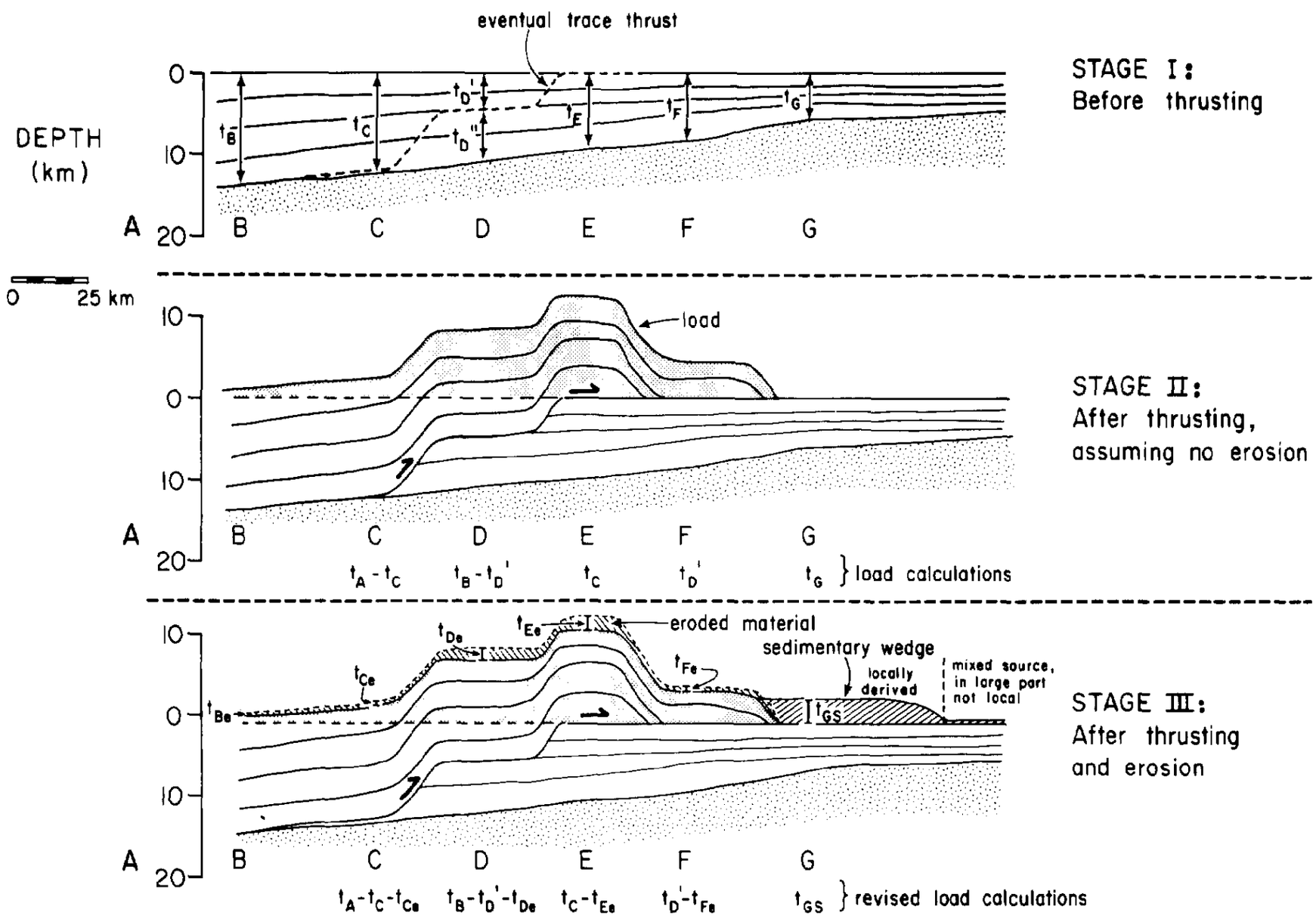

FIG. 13—Method of determining crustal load profiles for each thrust interval. Step I is pre-thrust geometry. During step II, section is duplicated by horizontal shortening. In step III, volume of sediments in thick western part of foreland basin is eroded from thrusts (see text). Loads of both thrusts and basin fill of step III are those used in computations.

Jordan, AAPG Bull, 1981

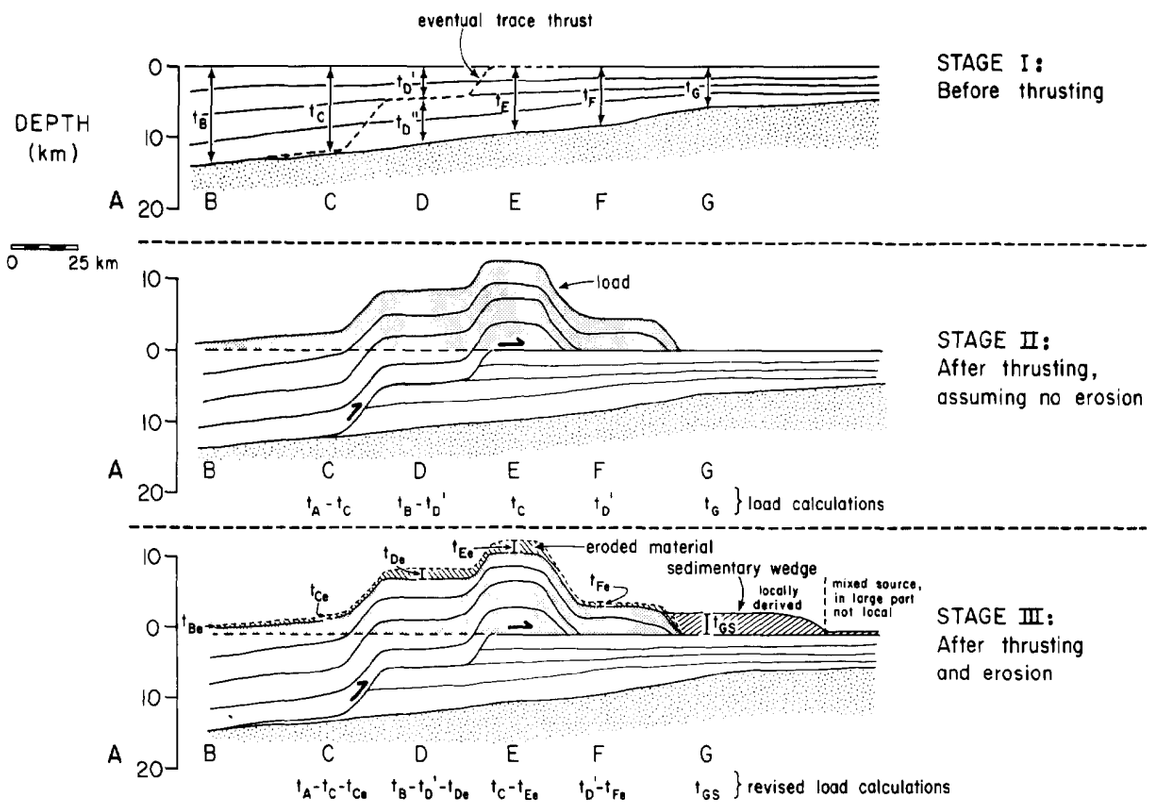

FIG. 13—Method of determining crustal load profiles for each thrust interval. Step I is pre-thrust geometry. During step II, section is duplicated by horizontal shortening. In step III, volume of sediments in thick western part of foreland basin is eroded from thrusts (see text). Loads of both thrusts and basin fill of step III are those used in computations.

Jordan, AAPG Bull, 1981

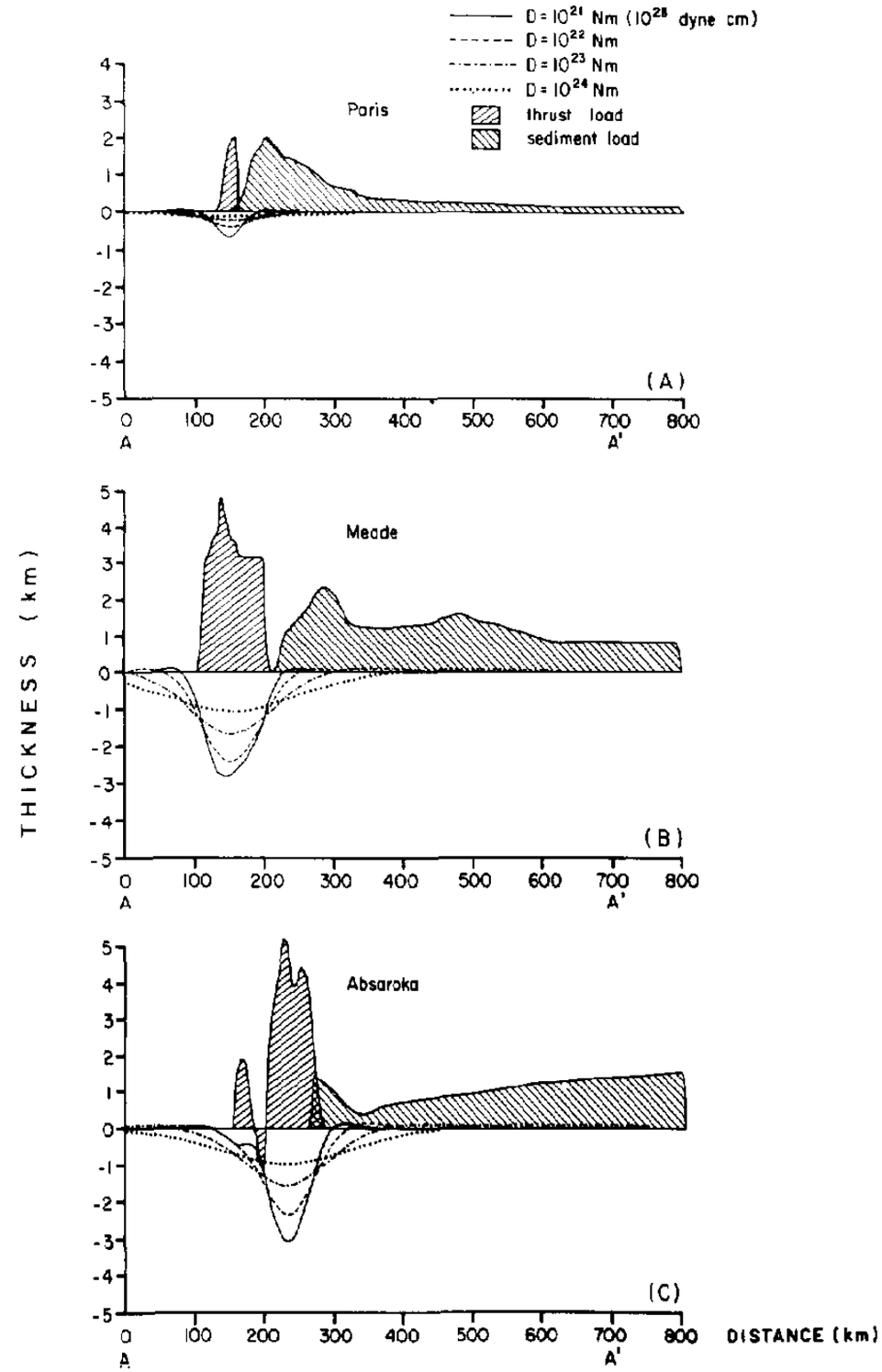

FIG. 14—Comparison of predicted crustal subsidence, due only to 3 thrust loads illustrated, to preserved thickness along AA′ for 4 values of flexural rigidity. Three time intervals are discriminated, corresponding to (A) Paris, (B) Meade, and (C) Absaroka thrusts. Palinspastic thickness of strata also illustrated. Prospect thrust on AA′ (Fig. 1) corresponds to 320 km. Vertical exaggeration 50:1.

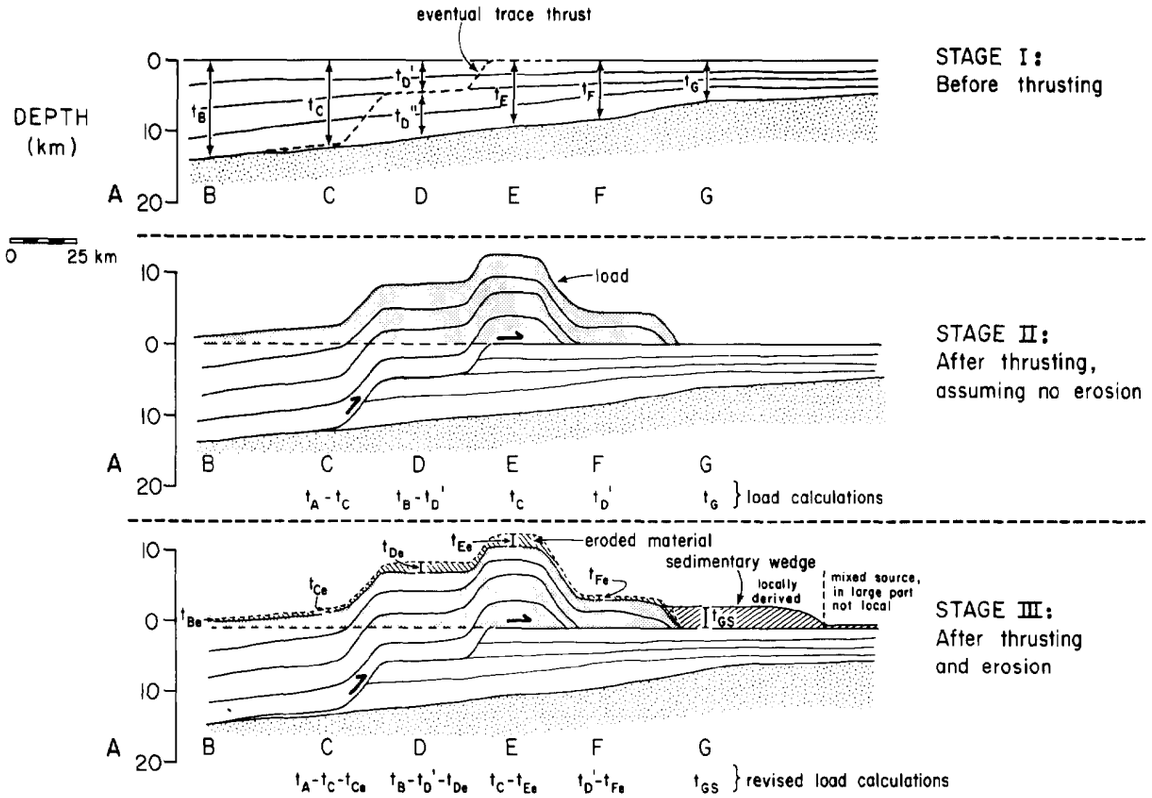

FIG. 13—Method of determining crustal load profiles for each thrust interval. Step I is pre-thrust geometry. During step II, section is duplicated by horizontal shortening. In step III, volume of sediments in thick western part of foreland basin is eroded from thrusts (see text). Loads of both thrusts and basin fill of step III are those used in computations.

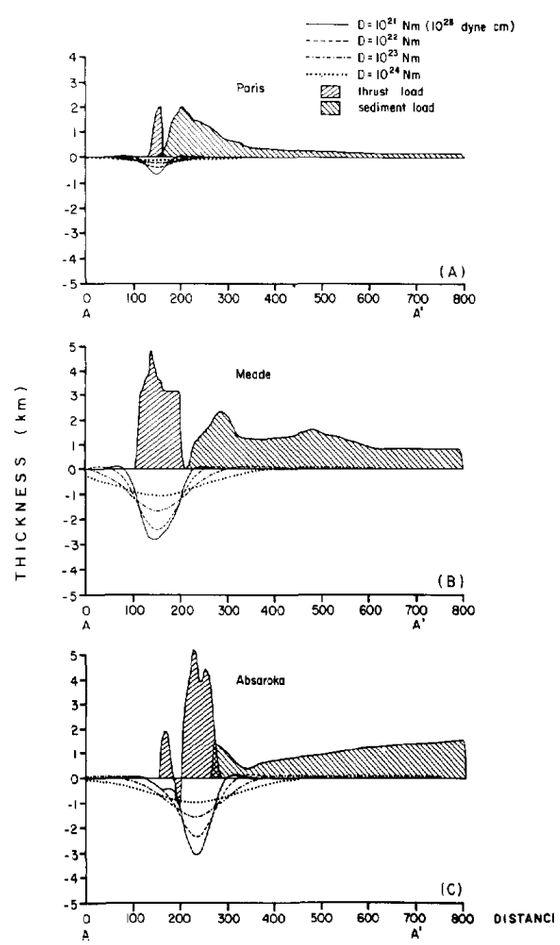

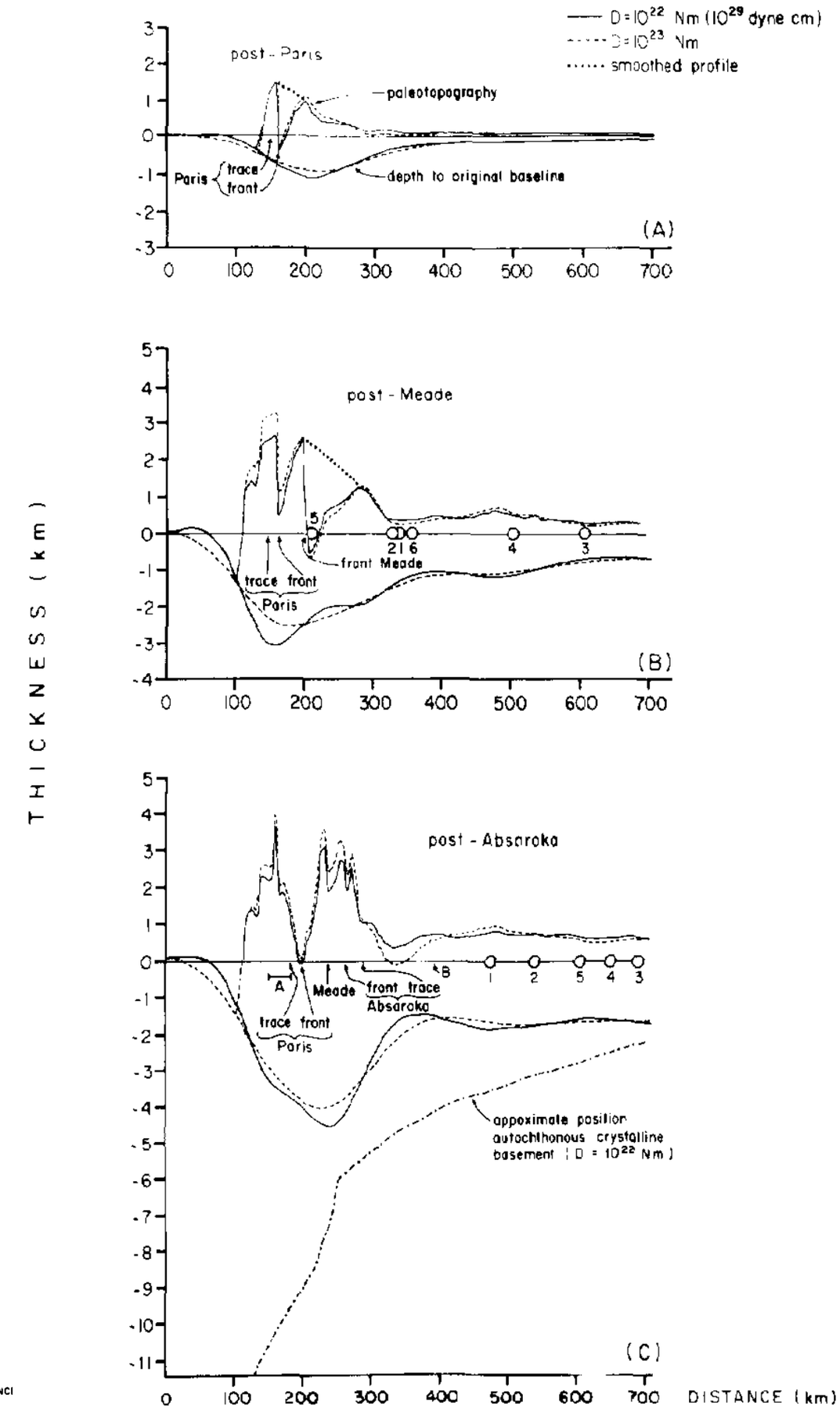

Jordan, AAPG Bull, 1981

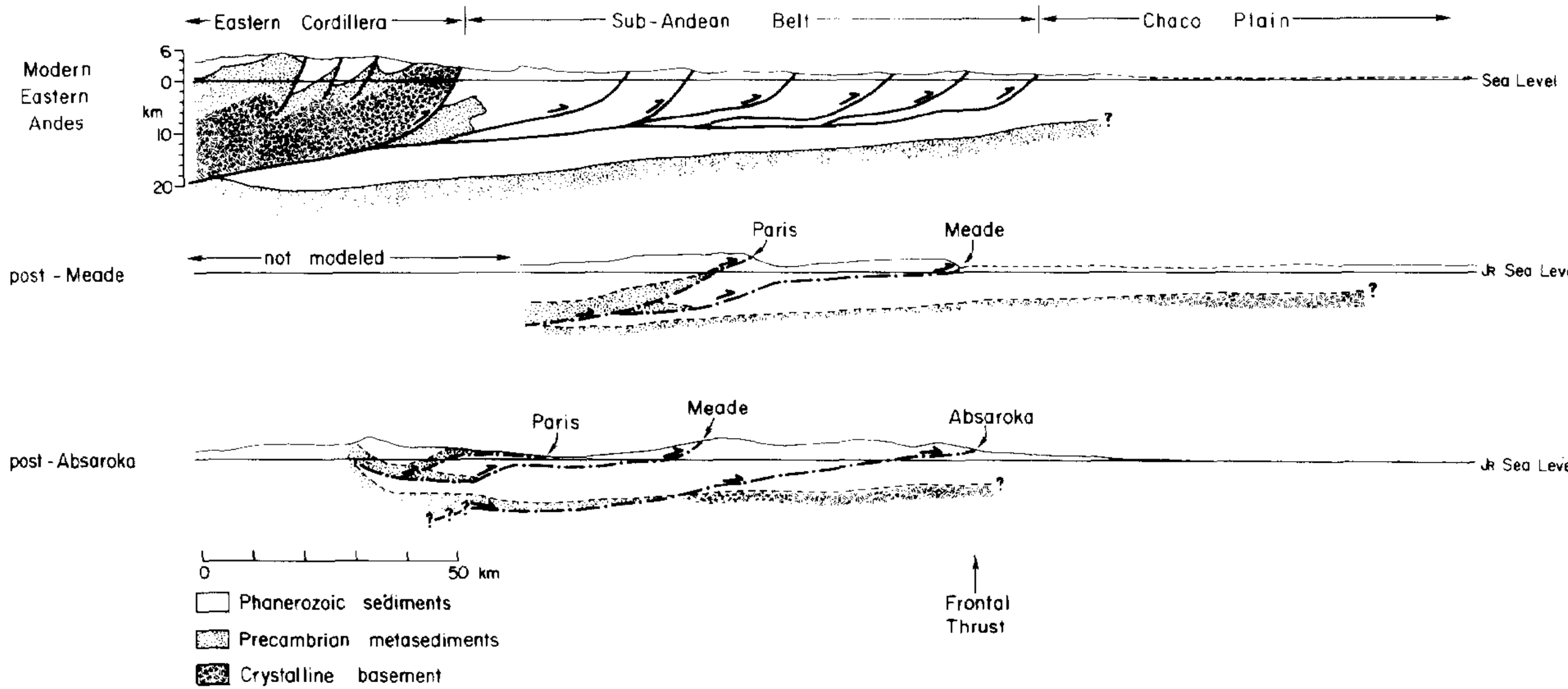

FIG. 16—Comparison of topography of modern Andean foreland thrust belt in northernmost Argentina (from Mingramm et al, 1979) to predicted post-Meade and post-Absaroka topography, showing morphologic segmentation. Meade and Absaroka profiles are shifted laterally to place coeval frontal thrust in line with active frontal thrust in Subandean belt. Andean geology and generalized reconstruction of Cretaceous subsurface geometry show tendency to expose older rocks in more interior part of thrust belt. No vertical exaggeration.

Jordan, AAPG Bull, 1981

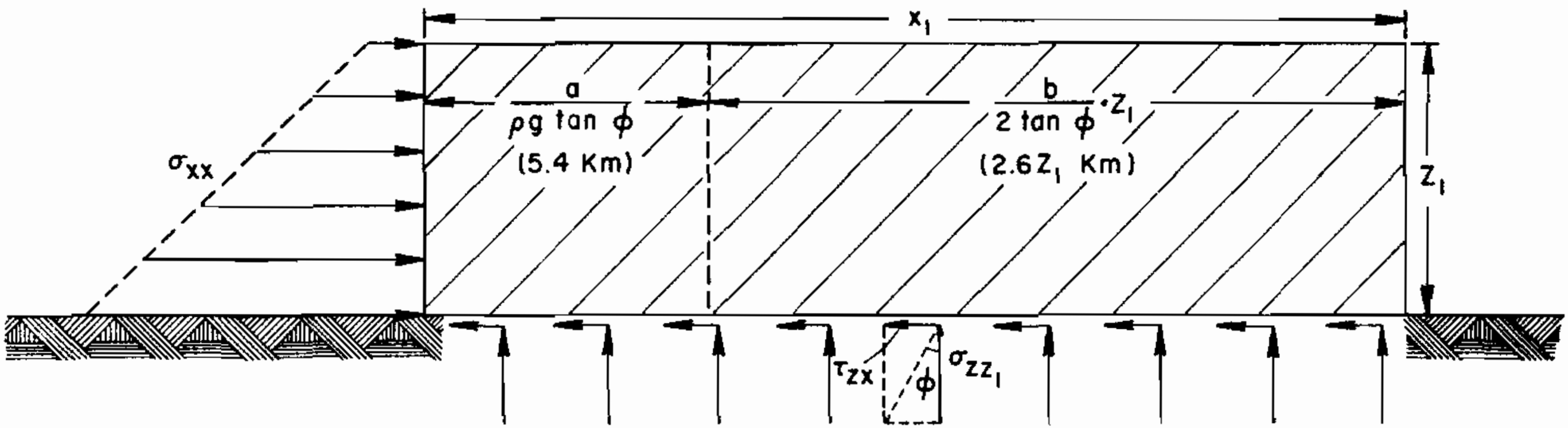

FIGURE 6.—ALGEBRAIC AND APPROXIMATE NUMERICAL VALUES OF THE TERMS OF EQUATION (15) FOR MAXIMUM LENGTH OF BLOCK

Hubbert & Rubey, GSA Bull, 1959

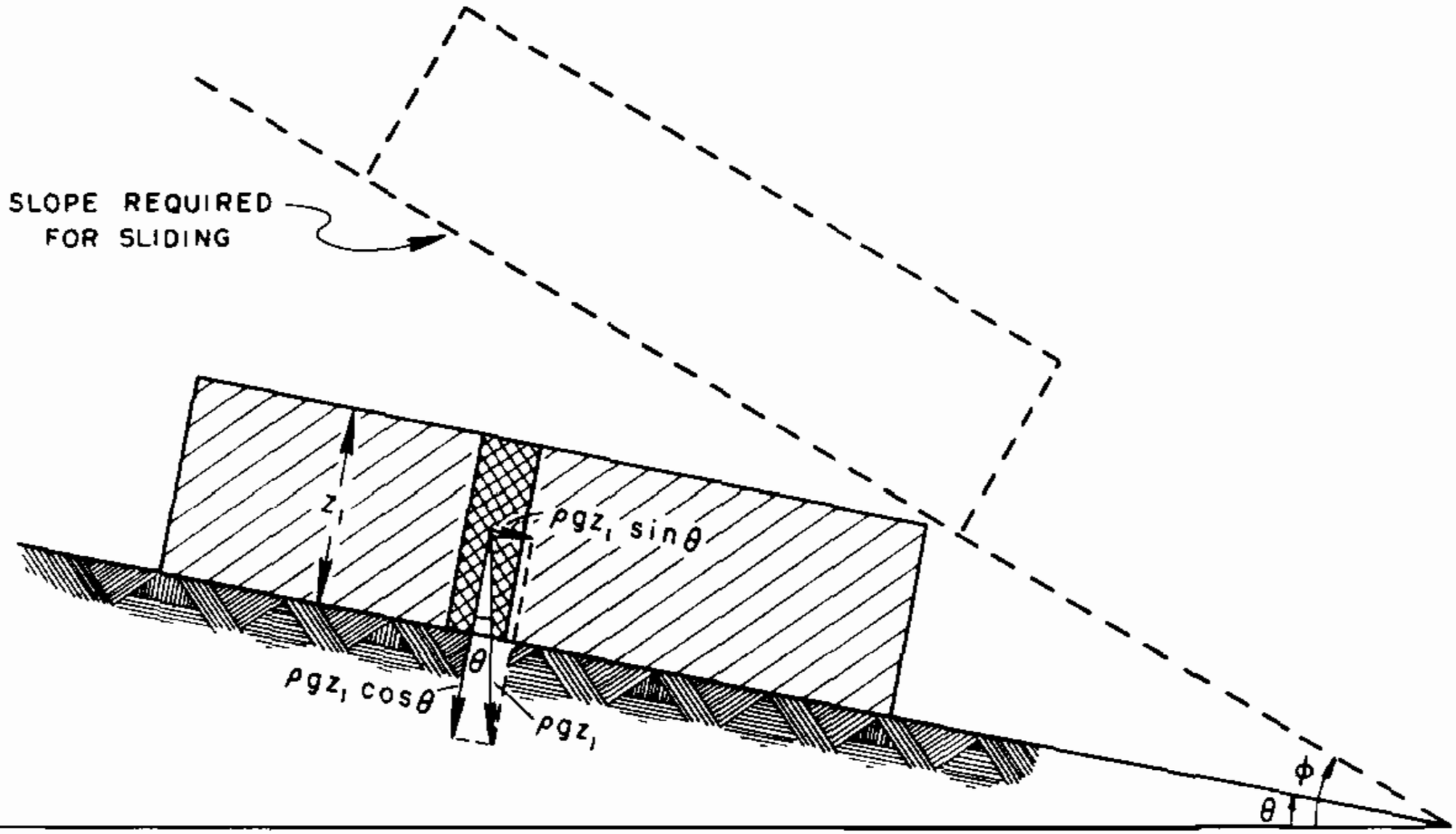

FIGURE 7.—NORMAL AND SHEAR STRESSES ON BASE OF BLOCK INCLINED AT ANGLE θ, AND ANGLE ϕ REQUIRED FOR SLIDING

Hubbert & Rubey, GSA Bull, 1959

λ_1 = ratio of pore pressure to lithostatic pressure

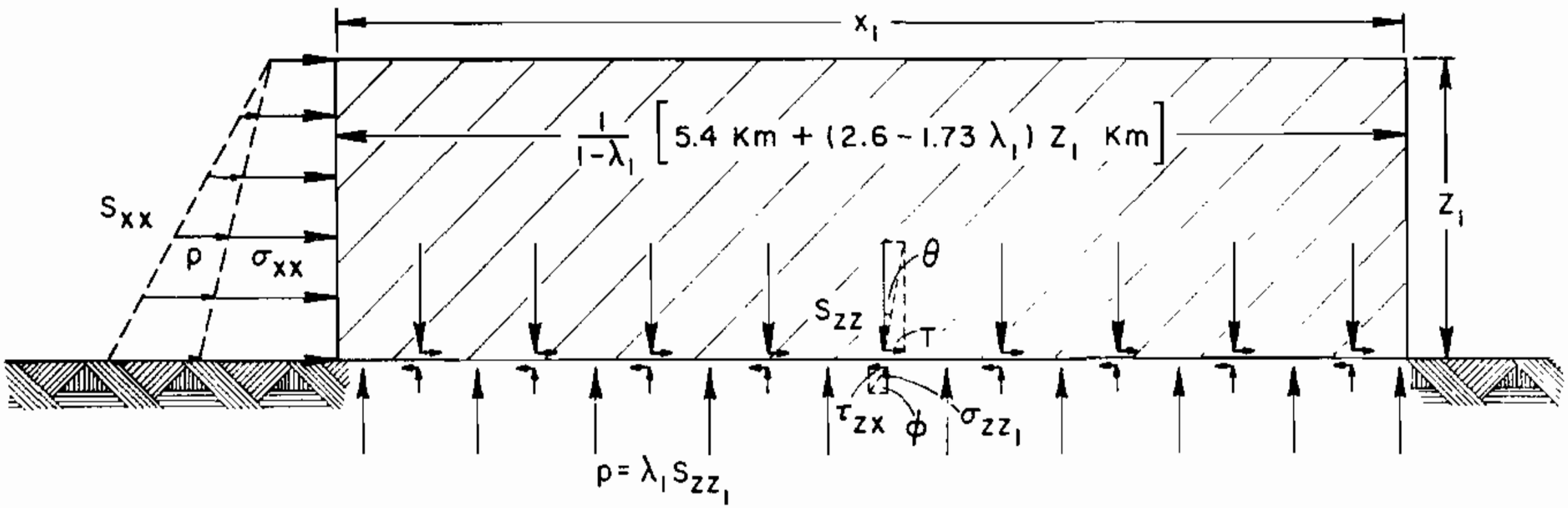

FIGURE 20.—MAXIMUM LENGTH OF HORIZONTAL BLOCK WITH INTERNAL FLUID PRESSURE WHICH CAN BE MOVED BY PUSH FROM REAR

Hubbert & Rubey, GSA Bull, 1959

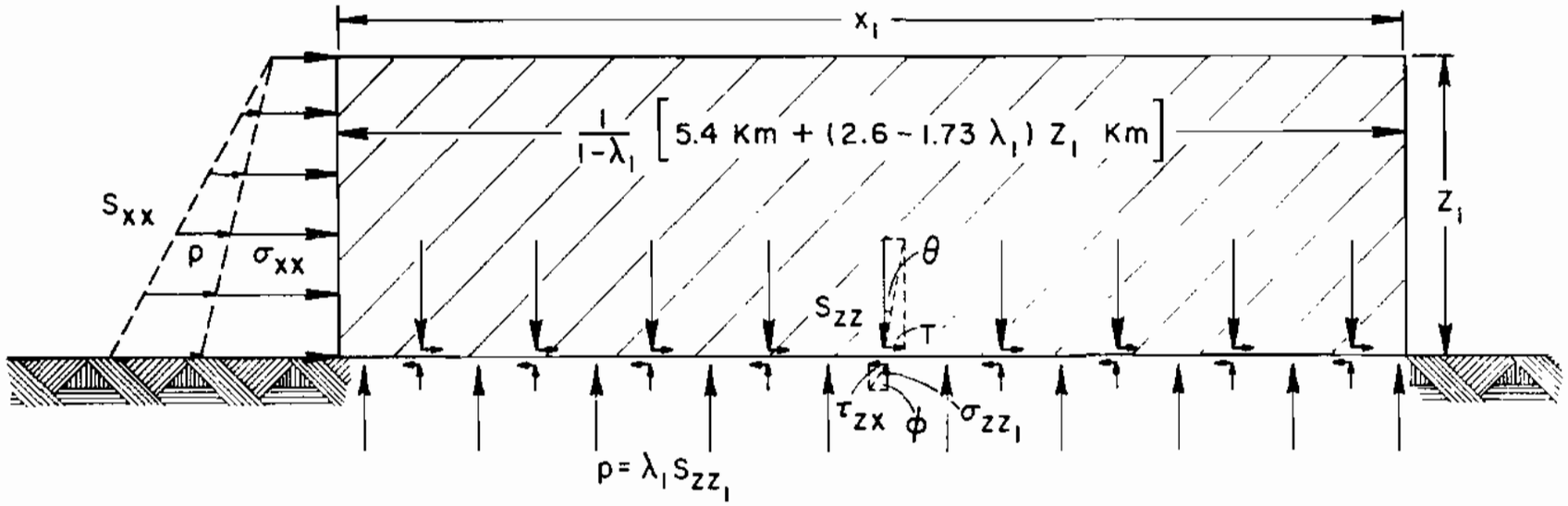

FIGURE 20.—MAXIMUM LENGTH OF HORIZONTAL BLOCK WITH INTERNAL FLUID PRESSURE WHICH CAN BE MOVED BY PUSH FROM REAR

λ_1 = ratio of pore pressure to lithostatic pressure

TABLE 1.—MAXIMUM LENGTH (IN KM) OF HORIZONTAL OVERTHRUST FOR VARIOUS THICKNESSES AND VALUES OF PRESSURE–OVERBURDEN RATIO

z_1 (km)	λ_1						
	0	0.465	0.5	0.6	0.7	0.8	0.9
1	8.0	13.4	14.2	17.3	22.5	32.9	64.0
2	10.6	16.7	17.6	21.2	27.1	39.0	74.4
3	13.2	20.1	21.1	25.1	31.8	45.1	84.8
4	15.8	23.5	24.6	29.0	36.4	51.2	95.2
5	18.4	26.8	28.0	32.9	41.0	57.3	106
6	21.0	30.2	31.5	36.8	45.6	63.4	116
7	23.6	33.6	34.9	40.7	50.3	69.5	126
8	26.2	36.9	38.4	44.6	54.9	75.6	137

Hubbert & Rubey, GSA Bull, 1959

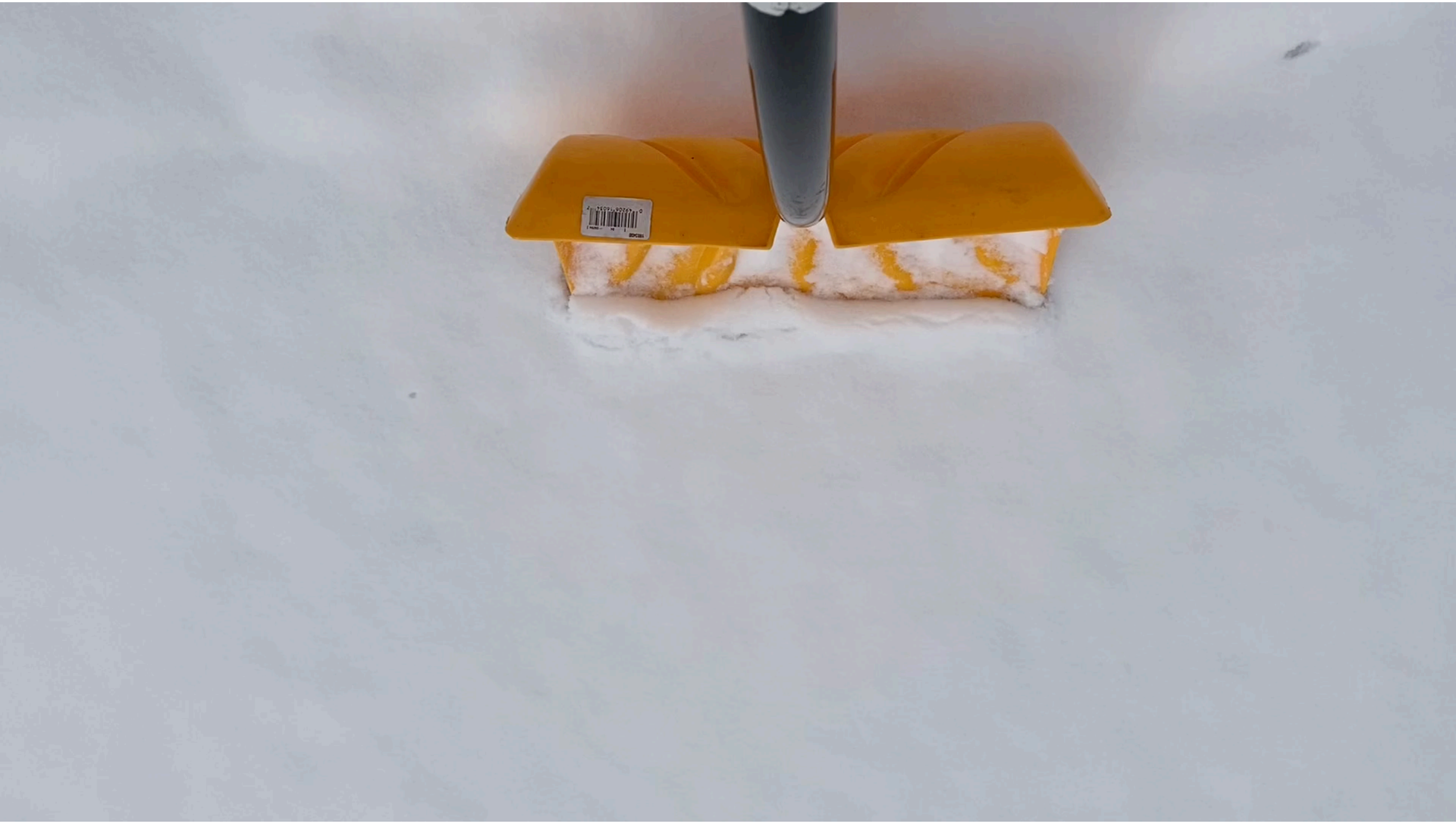

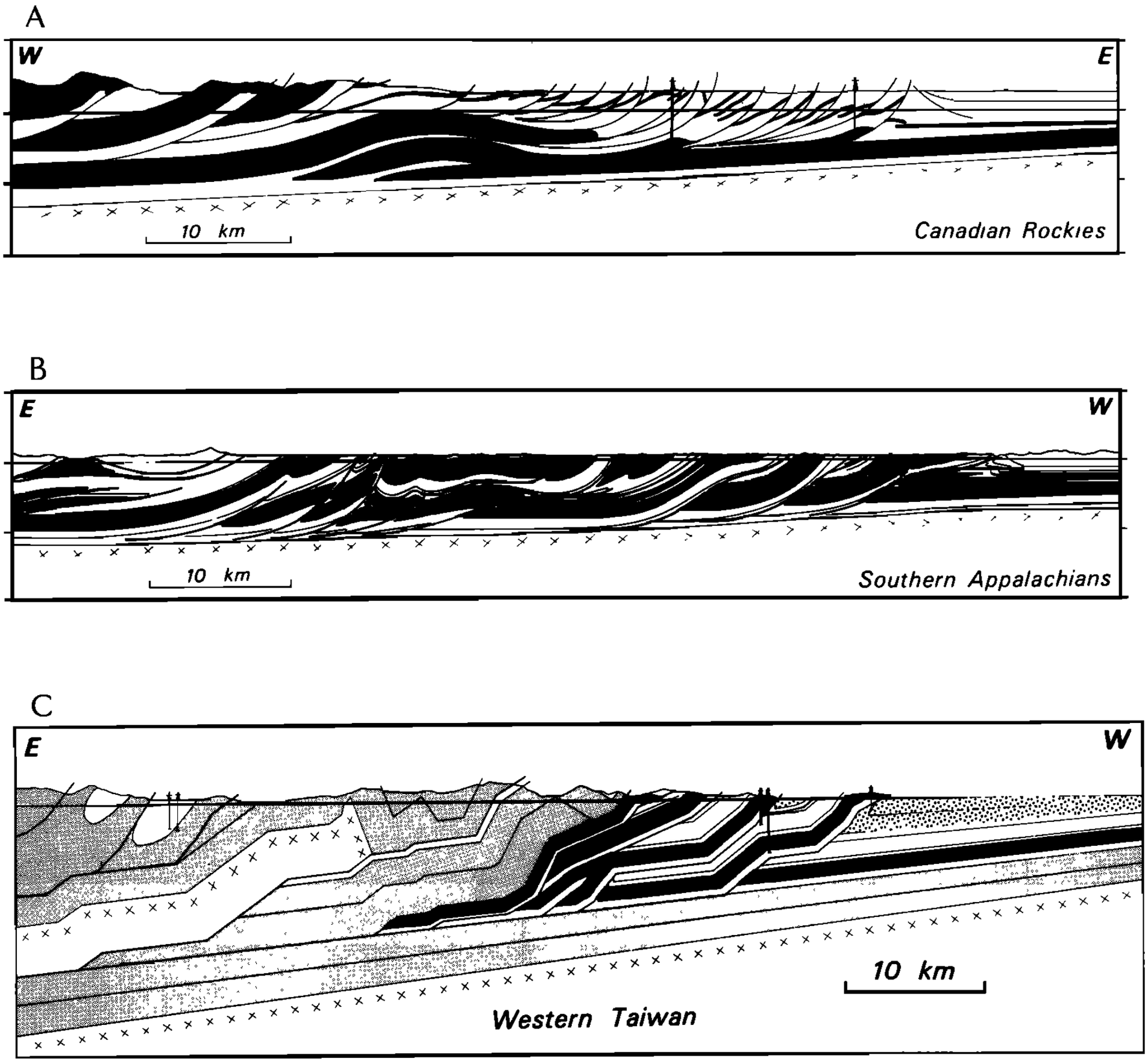

Fig. 1. Cross sections of several foreland fold-and-thrust belts: (*a*) Canadian Rockies [after *Bally et al.*, 1966], (*b*) southern Appalachians [after *Roeder et al.*, 1978], and (*c*) western Taiwan [after *Suppe*, 1980*a*].

Davis et al., JGR, 1984

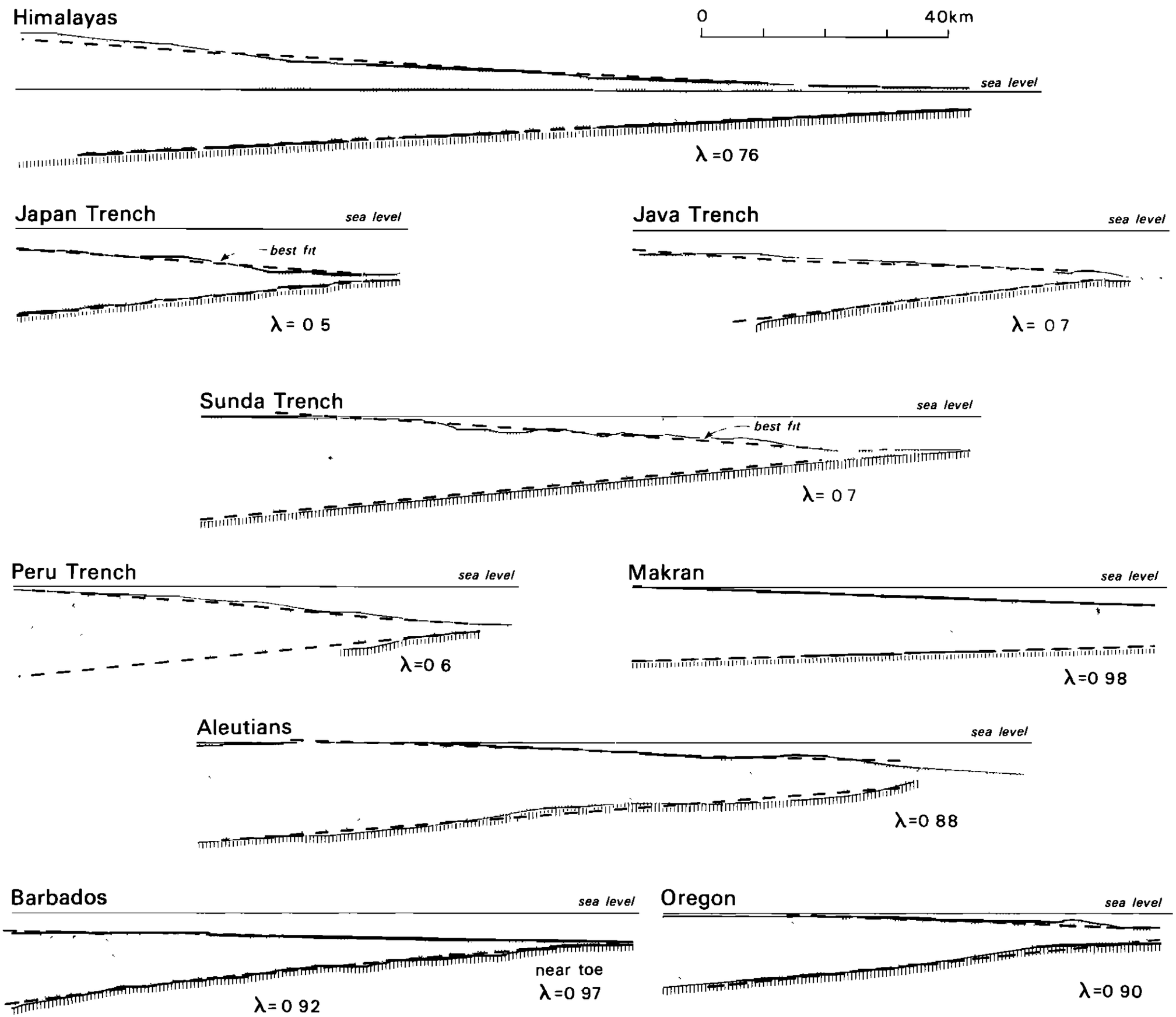

Fig. 16. Cross sections of the Himalayan fold-and-thrust belt and various active submarine accretionary wedges. Heavy dashed lines are best fitting linear profiles used to infer the fluid pressure ratios $\lambda = \lambda_b$, which are also shown.

Davis et al., JGR, 1984

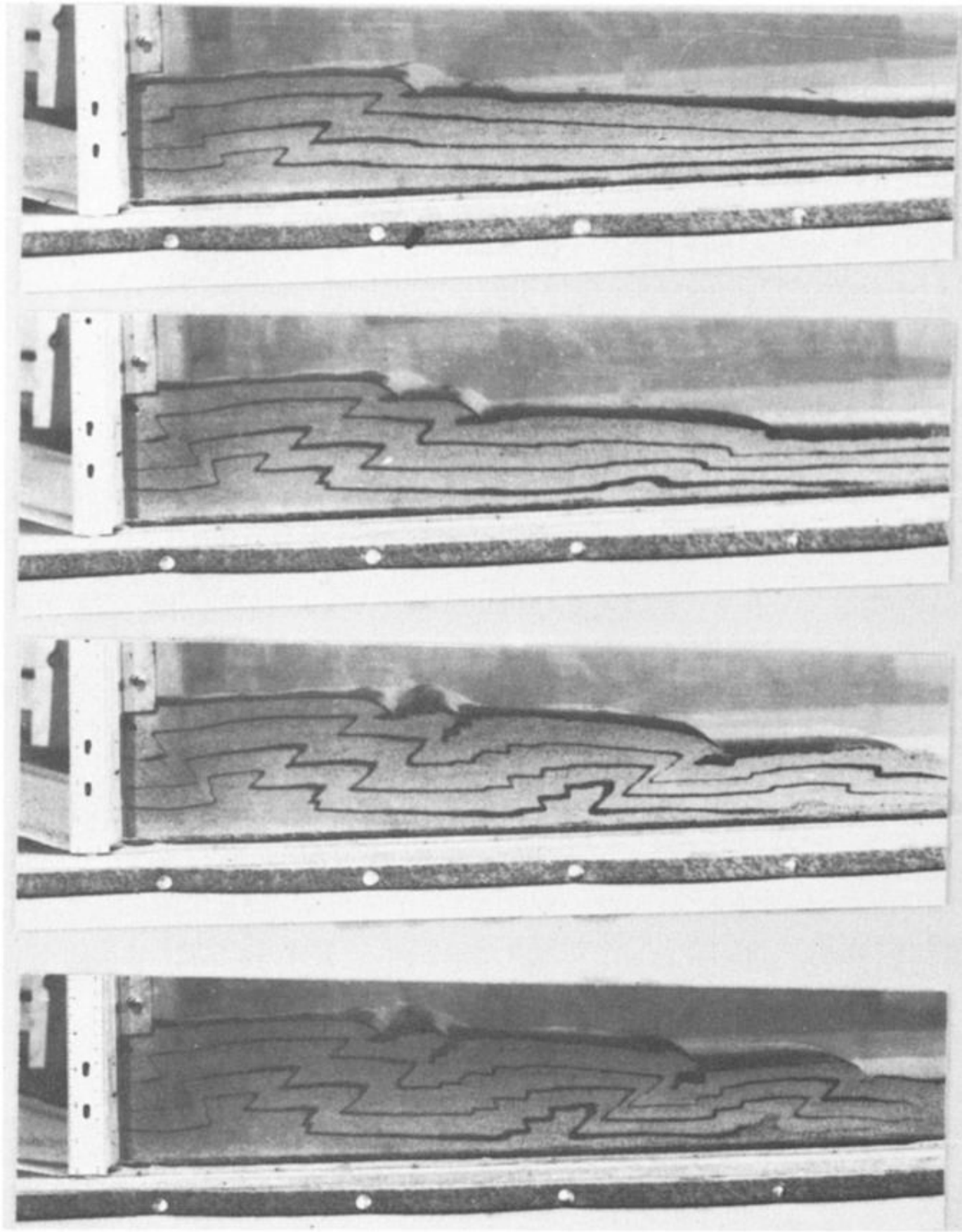

Fig. 3. Photographic side view of stages in deformation of sand during an experimental run. Initially undeformed sand mass is increasingly compressed and deformed by thrusting until the critical taper is attained. Black sand layers are passive markers.

Davis et al., JGR, 1984

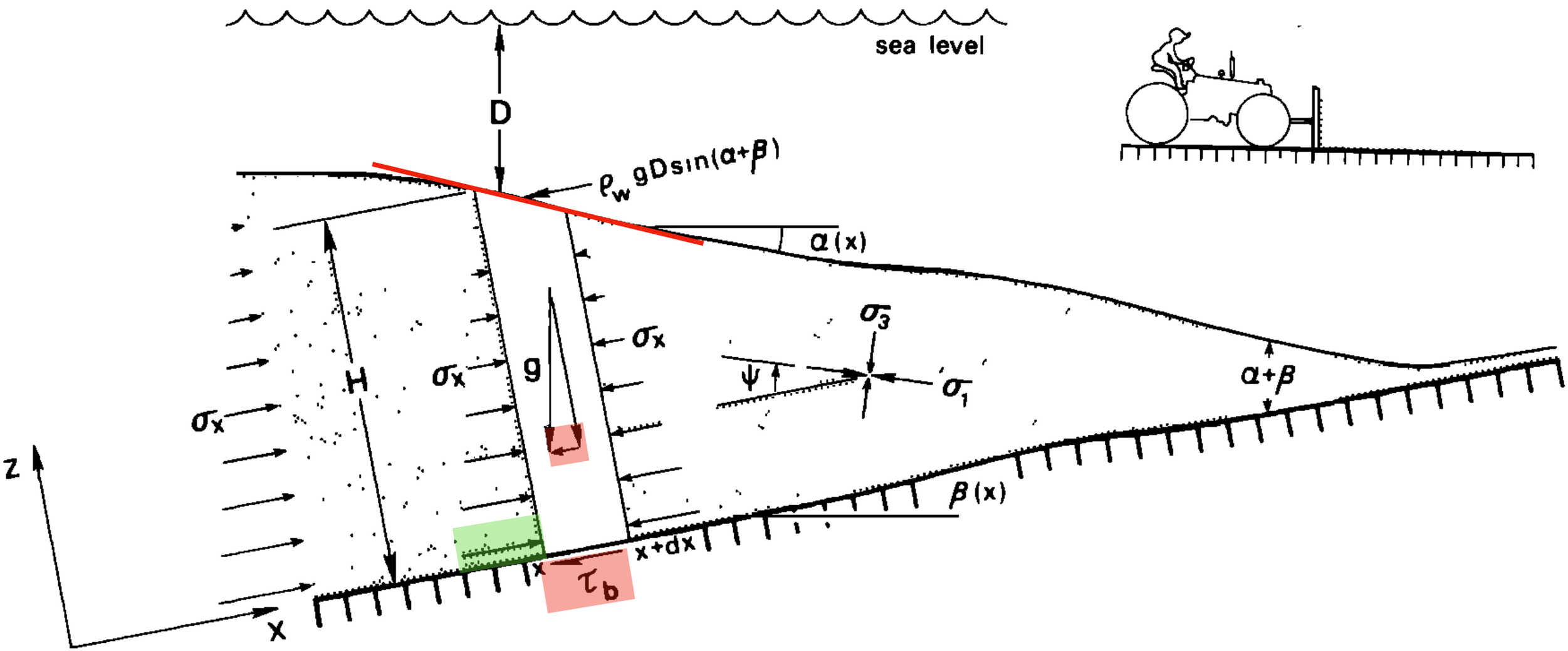

Fig. 5. Schematic diagram of a wedge of material subject to horizontal compression and on the verge of Coulomb failure throughout. The force balance on an arbitrary column of width *dx* is shown and the terminology used in deriving the equations of critical taper is indicated.

Davis et al., JGR, 1984

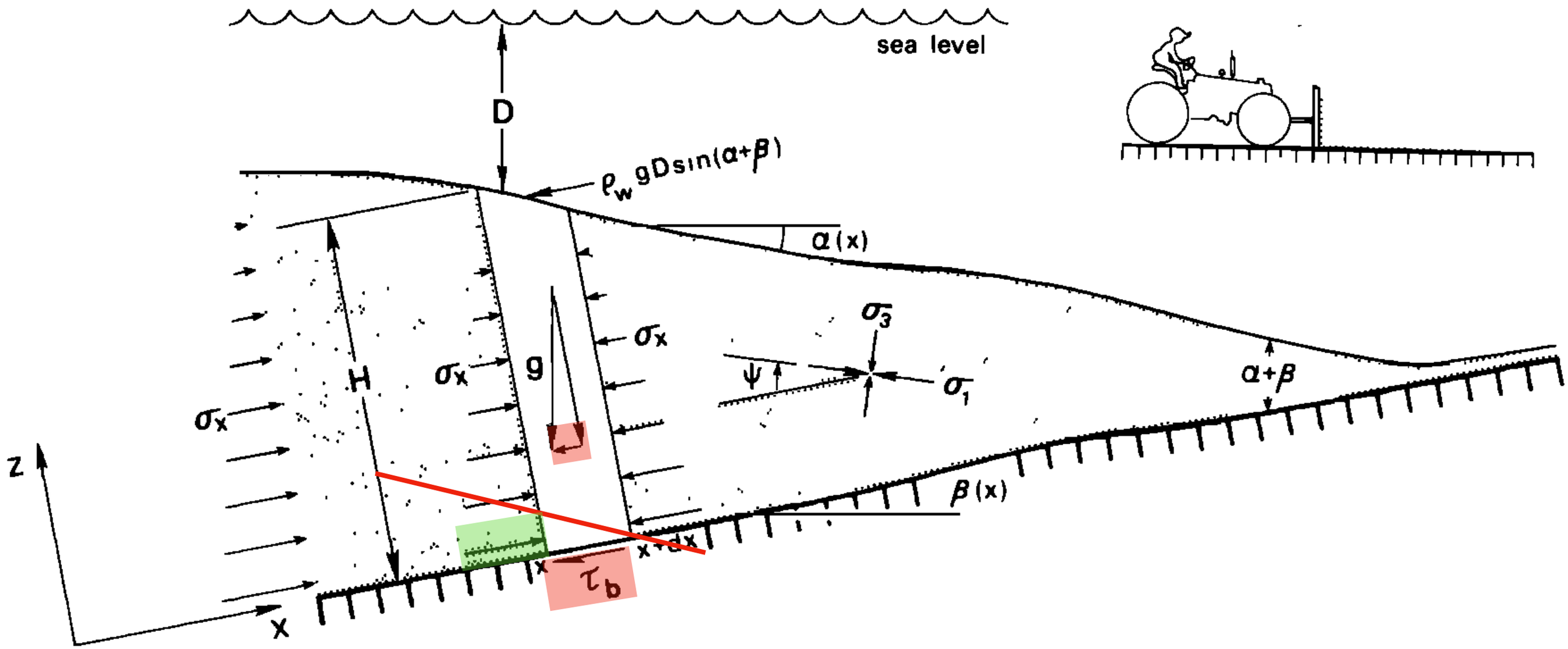

Fig. 5. Schematic diagram of a wedge of material subject to horizontal compression and on the verge of Coulomb failure throughout. The force balance on an arbitrary column of width *dx* is shown and the terminology used in deriving the equations of critical taper is indicated.

$$(\alpha+\beta)=\frac{\mu_b(1-\lambda_b)+\beta}{(q+\lambda(1-q))}$$

Davis et al., JGR, 1984

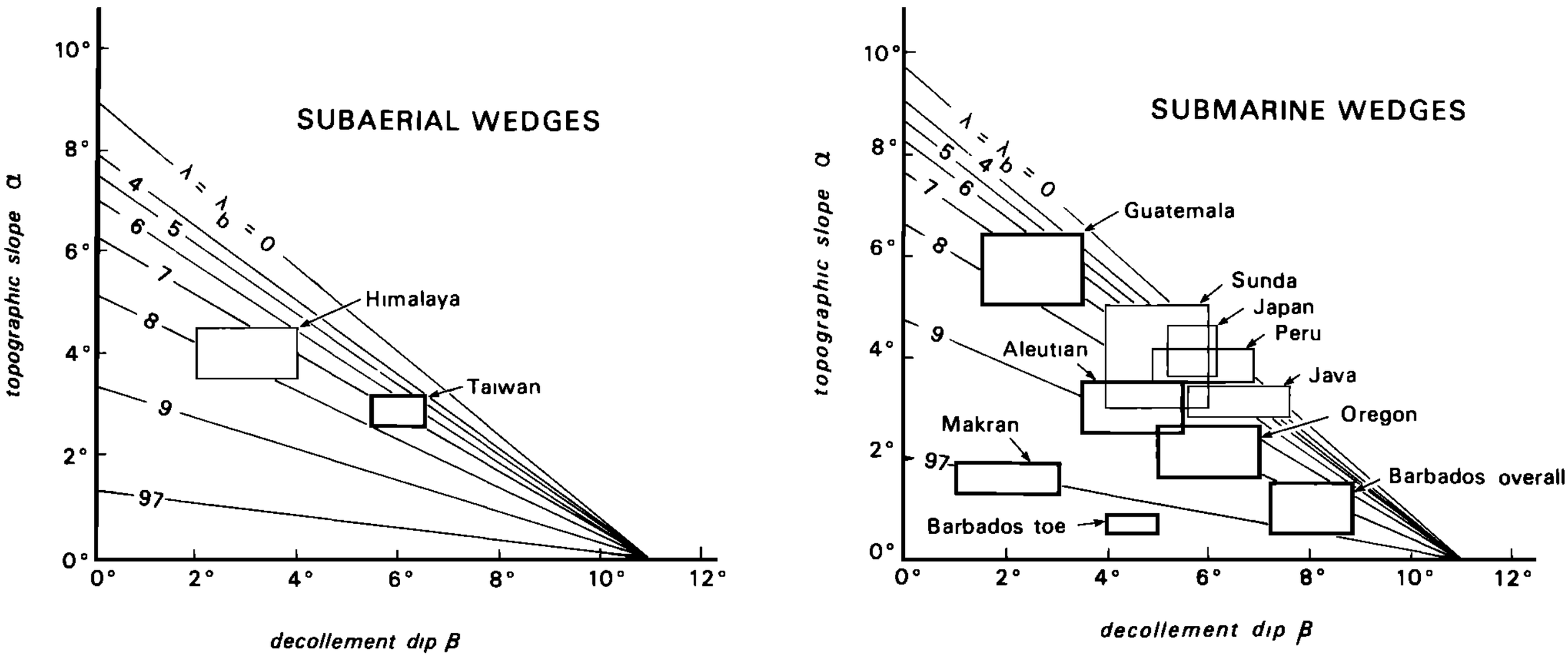

Fig. 17. Theoretical linear relationships $\alpha + R\beta = F$ for various fluid pressure ratios $\lambda = \lambda_b$, assuming $\mu_b = 0.85$ and $\mu = 1.03$. Boxes indicate observed geometries of active wedges, used to infer the fluid pressure ratios within them. Heavy outlines indicate those wedges for which some direct fluid pressure information is available. A rock density $\rho = 2.4$ g/cm^3 was used in the submarine case; other values would yield very similar results as the sensitivity to ρ is slight.

Davis et al., JGR, 1984

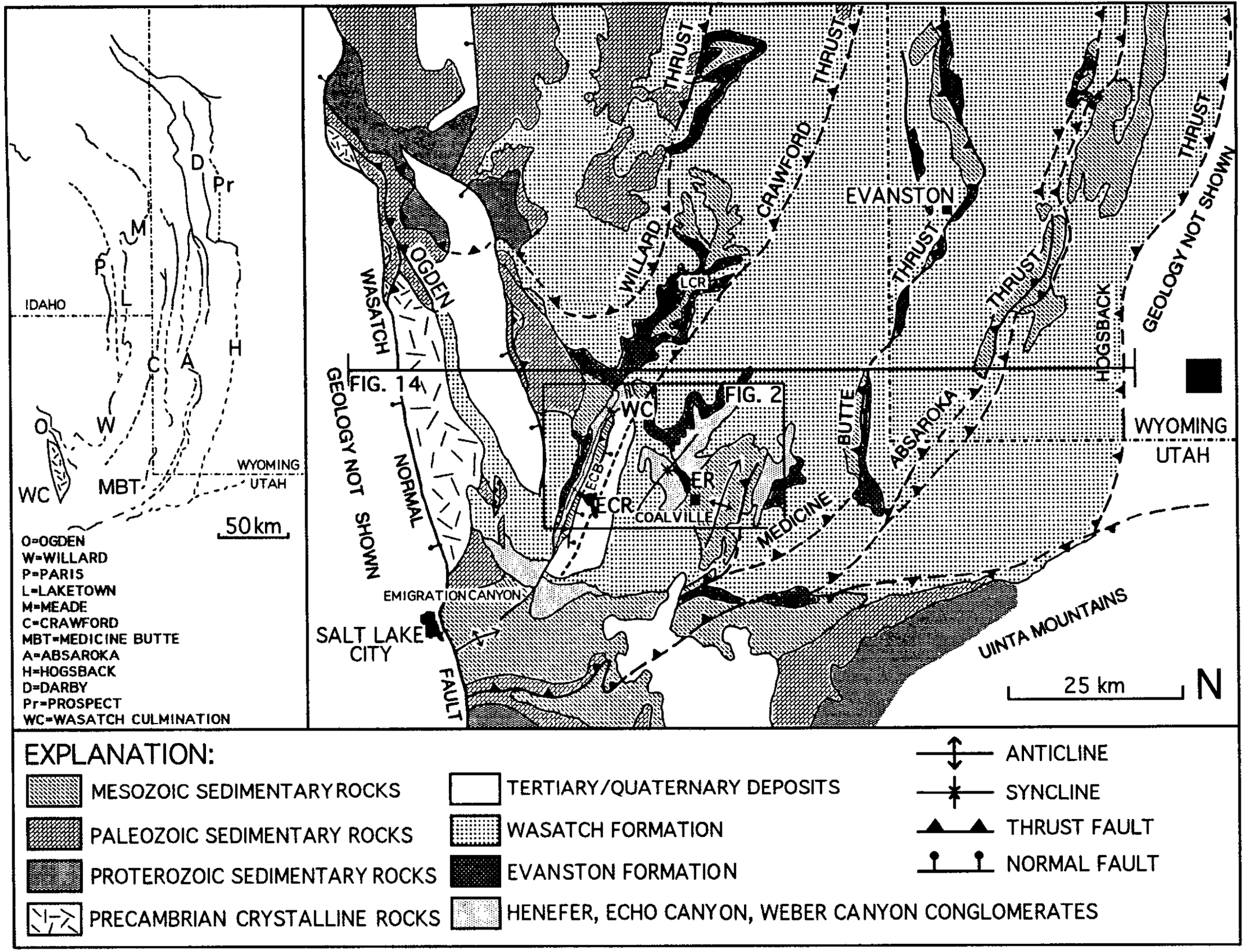

Figure 1. General map showing major structural features and bedrock geology of northeastern Utah and southwestern Wyoming, after Mullens (1971), Bryant (1990), and Yonkee (1992). Inset at left shows major thrust faults in Sevier belt in its Idaho-Wyoming-Utah salient, after Coogan (1992). Box near center of map indicates area shown in Figure 2. East-west line indicates approximate line of regional cross section discussed in text and in Figure 14. Black square east of Hogsback thrust indicates the Rock Springs, Wyoming, area. ECB, East Canyon backthrust; ECR, East Canyon Reservoir; WC, Weber Canyon; ER, Echo Reservoir; LCR, Lost Creek Reservoir.

DeCelles, GSA Bull, 1994

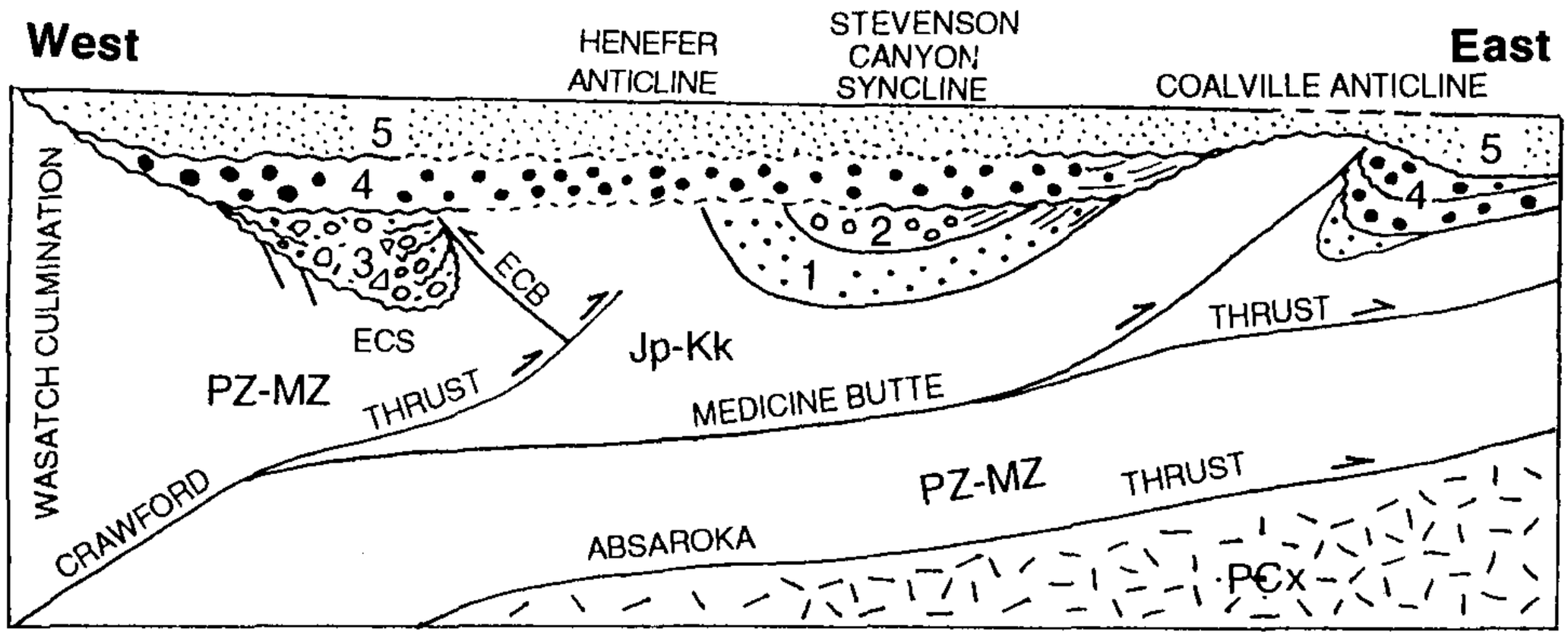

Figure 4. Schematic cross section illustrating the key structural and synorogenic stratigraphic relationships documented in the area between Weber Canyon and Coalville anticline (Fig. 2). The synorogenic conglomerate units are numbered in order of decreasing age: 1, Henefer Formation; 2, Echo Canyon Conglomerate; 3, Weber Canyon Conglomerate; 4, Evanston Formation; 5, Wasatch Formation. ECS = East Canyon syncline; ECB = East Canyon backthrust; Jp-Kk = Jurassic–Lower Cretaceous Preuss and Kelvin Formations; PZ-MZ = Paleozoic through Middle Jurassic rocks; P€x = Precambrian crystalline basement. Relationships on east side of Coalville anticline are from Lamerson (1982). Note that the Weber Canyon Conglomerate is incorporated into a growth syncline in the footwall of the East Canyon backthrust and Henefer anticline, whereas the Henefer and Echo Canyon contain no evidence of syndepositional growth of Henefer anticline.

DeCelles, GSA Bull, 1994

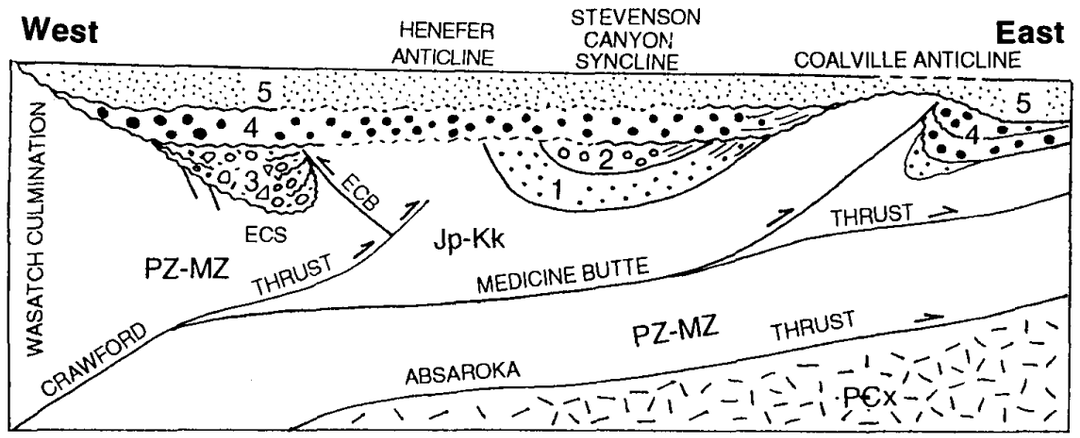

Figure 4. Schematic cross section illustrating the key structural and synorogenic stratigraphic relationships documented in the area between Weber Canyon and Coalville anticline (Fig. 2). The synorogenic conglomerate units are numbered in order of decreasing age: 1, Henefer Formation; 2, Echo Canyon Conglomerate; 3, Weber Canyon Conglomerate; 4, Evanston Formation; 5, Wasatch Formation. ECS = East Canyon syncline; ECB = East Canyon backthrust; Jp-Kk = Jurassic–Lower Cretaceous Preuss and Kelvin Formations; PZ-MZ = Paleozoic through Middle Jurassic rocks; P€x = Precambrian crystalline basement. Relationships on east side of Coalville anticline are from Lamerson (1982). Note that the Weber Canyon Conglomerate is incorporated into a growth syncline in the footwall of the East Canyon backthrust and Henefer anticline, whereas the Henefer and Echo Canyon contain no evidence of syndepositional growth of Henefer anticline.

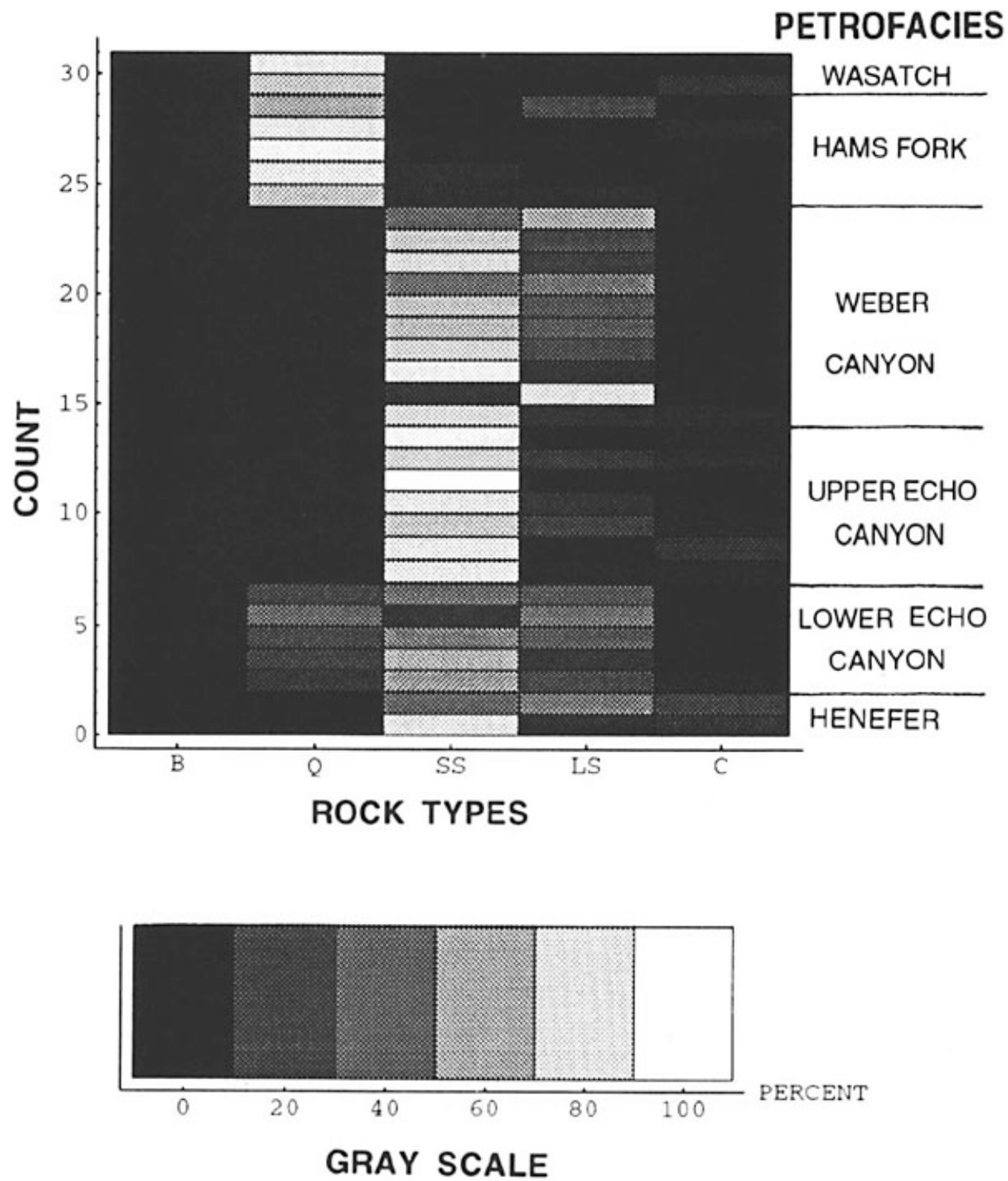

Figure 11. (Top) *Mathematica* density plot of normalized clast-count data from the Upper Cretaceous–Paleocene synorogenic conglomerates of northeast Utah and southwest Wyoming; (below) gray scale. Vertical axis in density plot represents the number of the clast count in stratigraphically ascending order, and rock types are listed along the horizontal axis. Rock-type symbols are as follows: B, crystalline basement rocks; Q, Proterozoic quartzite; SS, Paleozoic and Mesozoic quartzite, sandstone, and siltstone; LS, limestone and dolomite; C, chert. Conglomerate petrofacies from which the data were collected are listed along the right side. Gray levels indicate clast abundance, with white indicating 100% and black indicating 0%. For example, clast-count 1 is from the Henefer Formation and contains no crystalline basement and quartzite clasts, minor amounts of limestone and chert, and abundant Paleozoic and Mesozoic sandstone and siltstone.

DeCelles, GSA Bull, 1994

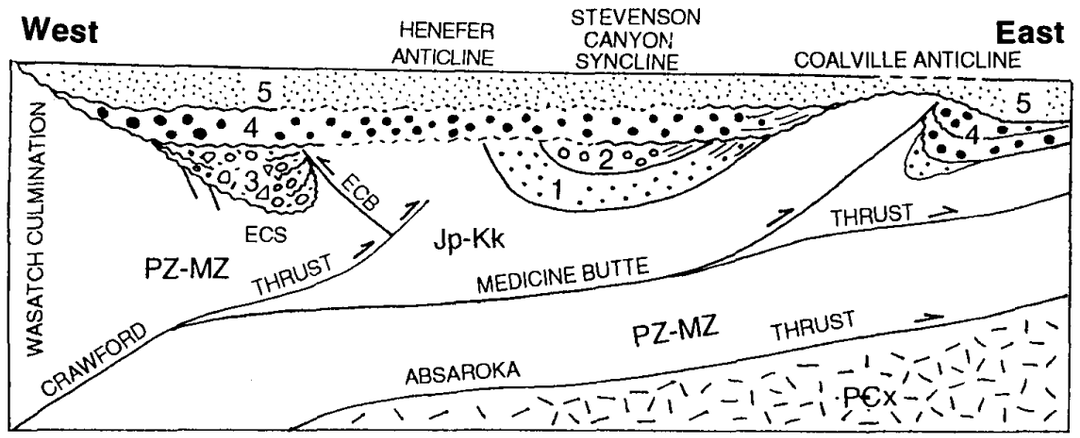

Figure 4. Schematic cross section illustrating the key structural and synorogenic stratigraphic relationships documented in the area between Weber Canyon and Coalville anticline (Fig. 2). The synorogenic conglomerate units are numbered in order of decreasing age: 1, Henefer Formation; 2, Echo Canyon Conglomerate; 3, Weber Canyon Conglomerate; 4, Evanston Formation; 5, Wasatch Formation. ECS = East Canyon syncline; ECB = East Canyon backthrust; Jp-Kk = Jurassic–Lower Cretaceous Preuss and Kelvin Formations; PZ-MZ = Paleozoic through Middle Jurassic rocks; P€x = Precambrian crystalline basement. Relationships on east side of Coalville anticline are from Lamerson (1982). Note that the Weber Canyon Conglomerate is incorporated into a growth syncline in the footwall of the East Canyon backthrust and Henefer anticline, whereas the Henefer and Echo Canyon contain no evidence of syndepositional growth of Henefer anticline.

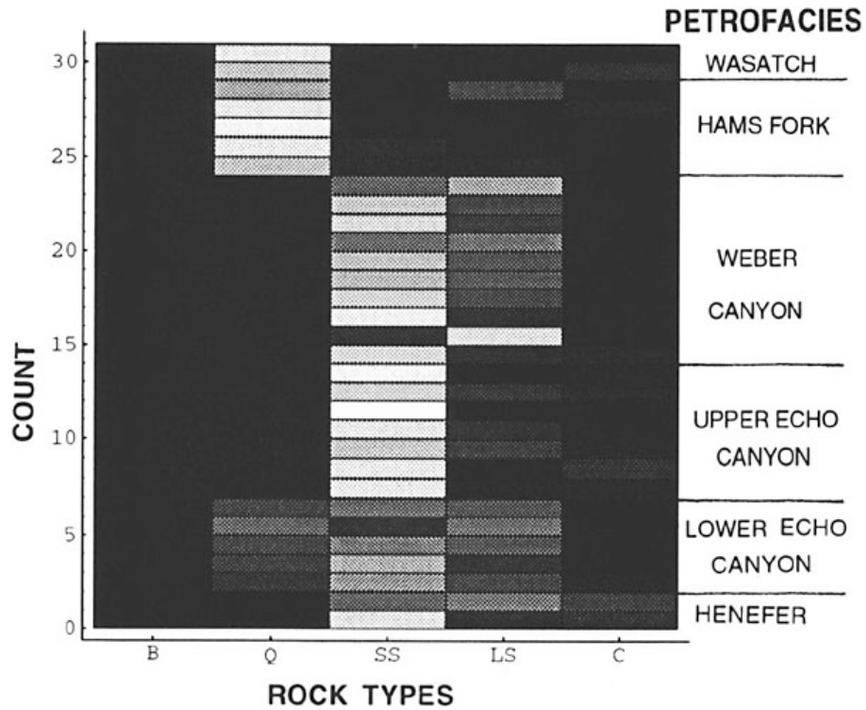

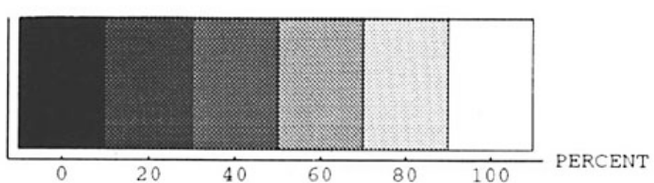

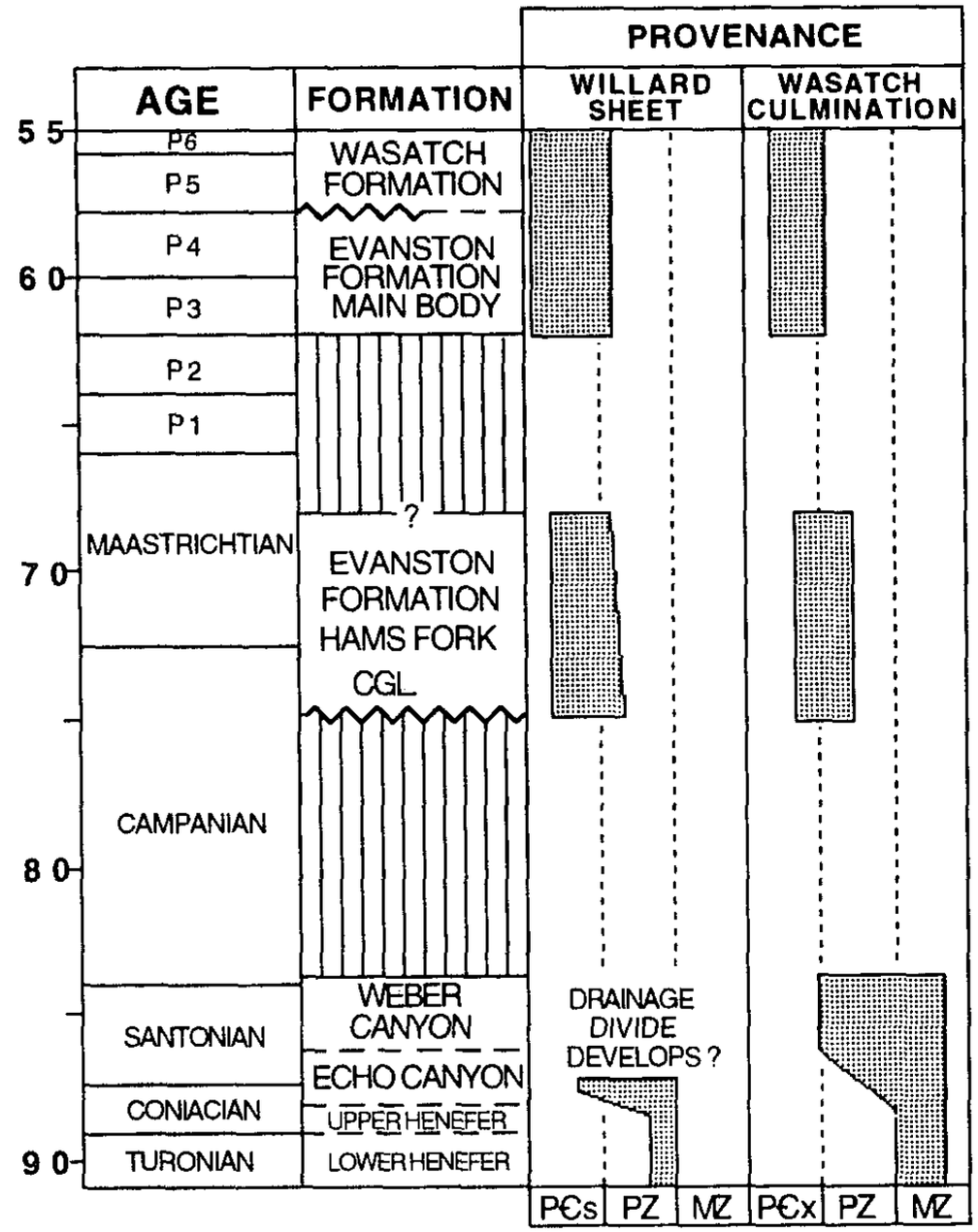

Figure 12. Plot showing the provenance of Upper Cretaceous–Paleocene synorogenic conglomerates in the study area. Sources are divided into those in the Willard thrust sheet and those in the eastern limb of the Wasatch culmination. Shaded areas represent the parts of the stratigraphic section that were exposed during deposition of the corresponding conglomerate. Symbols of rock units are as follows: P€s, Proterozoic sedimentary rocks; P€x, Precambrian crystalline basement rocks; PZ, Paleozoic sedimentary rocks; MZ, Mesozoic sedimentary rocks.

DeCelles, GSA Bull, 1994

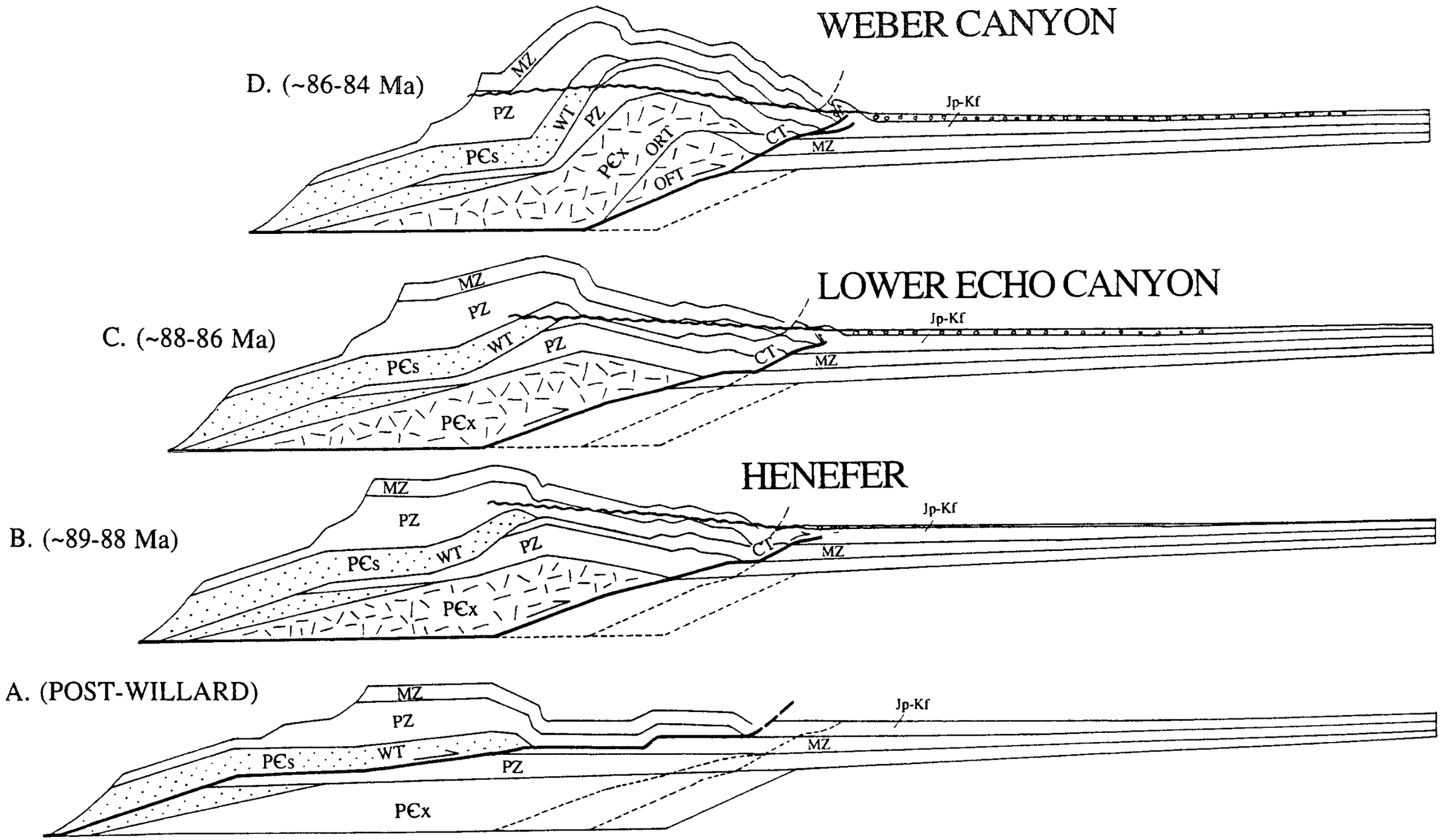

Figure 14. Sequential restoration of a regional cross section (see Fig. 1 for approximate location) from the Wasatch culmination and the Willard thrust sheet (on the west) to the Hogsback thrust fault (on the east). Stippled areas represent Proterozoic sedimentary rocks; jackstraw pattern represents Precambrian crystalline basement rocks. Open circle pattern indicates Upper Cretaceous–Paleocene synorogenic sediment (not included in balancing procedures). Symbols: P€x, Precambrian crystalline rocks; P€s, Proterozoic sedimentary rocks; PZ, Paleozoic; MZ, Triassic through Middle Jurassic (up to top of Twin Creek Formation); Jp-Kf, Upper Jurassic–Lower Cretaceous Preuss, Kelvin, and Frontier Formations; WT, Willard thrust; ORT, Ogden roof thrust; OFT, Ogden floor thrust; CT, Crawford thrust; MBT, Medicine Butte thrust; AT, Absaroka thrust; HT, Hogsback thrust. Cross sections are drawn so that a gently eastward-dipping (<4°) surface would expose the rocks necessary to account for the compositions of synorogenic conglomerates. See text for explanation. Modified from Yonkee (1992) and Coogan (1992).

DeCelles, GSA Bull, 1994

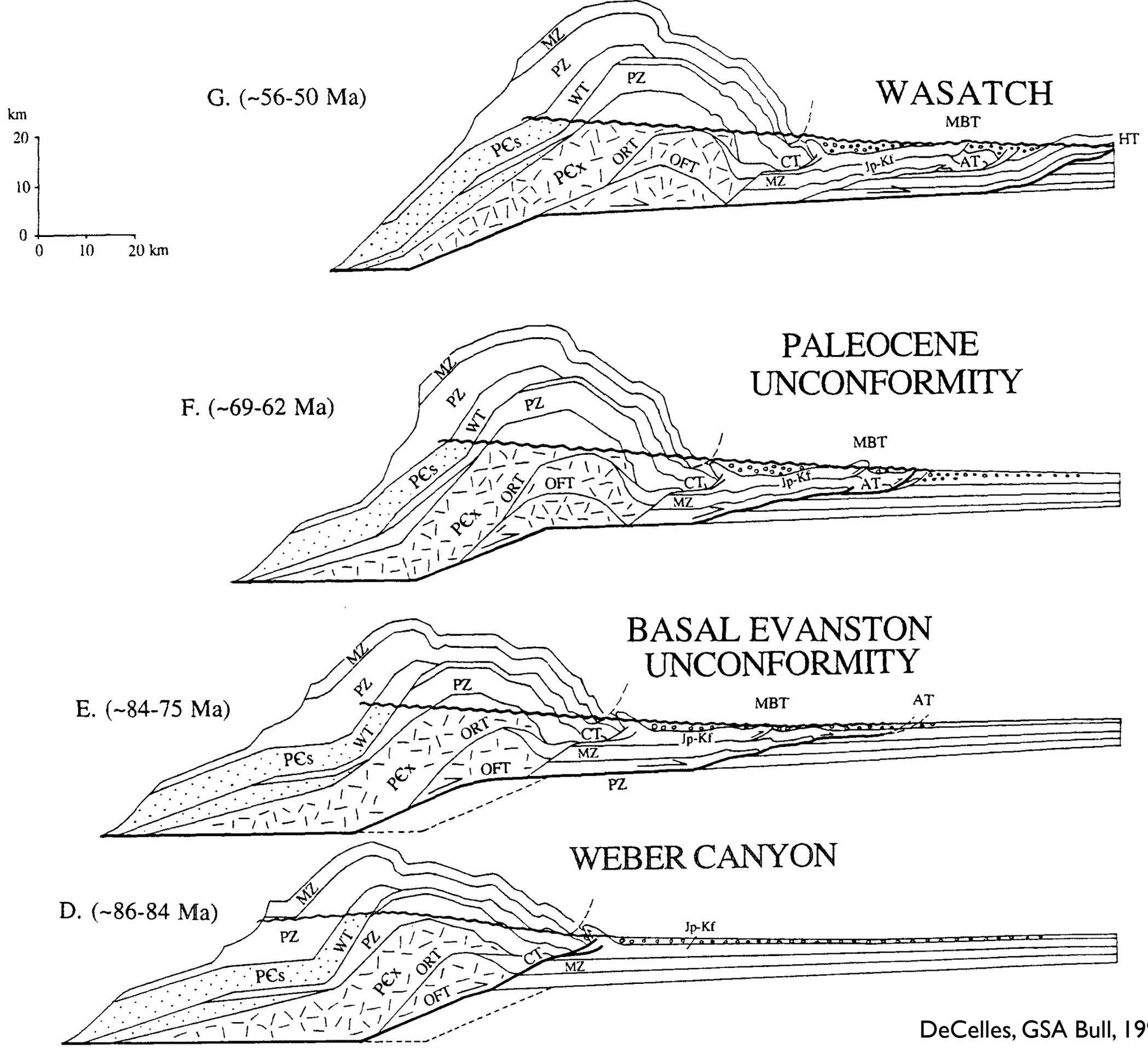

DeCelles, GSA Bull, 1994

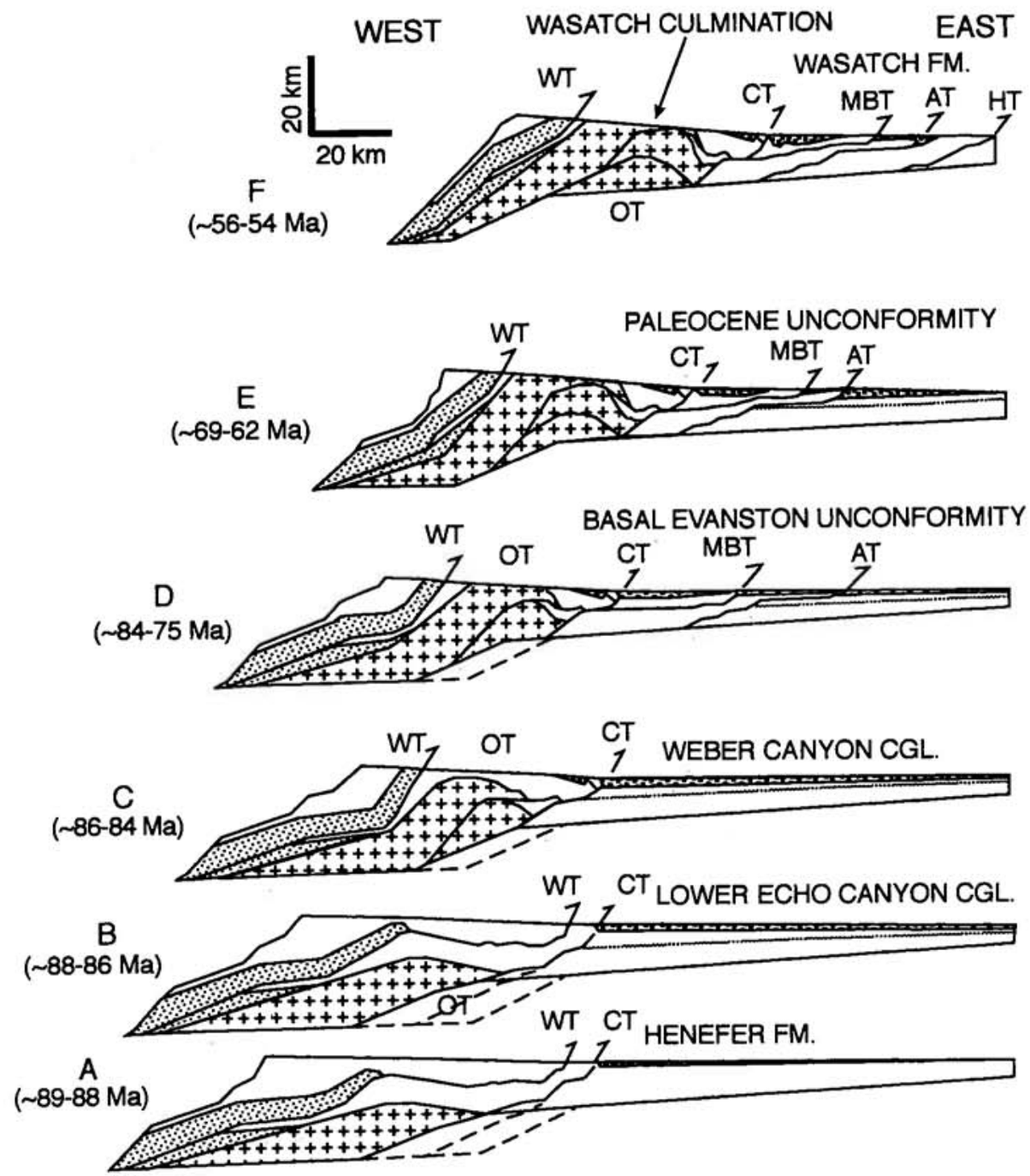

Figure 2. Incrementally restored regional cross section of the northeast Utah–southwest Wyoming part of the Sevier thrust belt, showing Late Cretaceous through Paleocene thrusting (after Yonkee, 1992, and Coogan, 1992a; see Fig. 1B for line of section). Restoration is defined by crosscutting structural relationships, synorogenic conglomerate provenance, and paleontological and radiometric dates summarized in DeCelles (1994). Plus sign pattern indicates Precambrian basement rocks; fine stipple is Proterozoic sedimentary and metasedimentary rocks; blank areas are Paleozoic through Upper Jurassic cover rocks; and coarse stipple represents Upper Cretaceous synorogenic sedimentary rocks. The shaded lines in B–E represent the level of Jurassic salt-bearing rocks. Thrust faults are labeled as follows: WT, Willard thrust; OT, Ogden thrust system, which involves several basement-involved thrusts; CT, Crawford thrust; MBT, Medicine Butte thrust; AT, Absaroka thrust; HT, Hogsback thrust. Note that the slopes of the basal décollement and upper topographic surface are not quantitatively constrained, as discussed in the text.

DeCelles & Mitra, GSA Bull, 1995

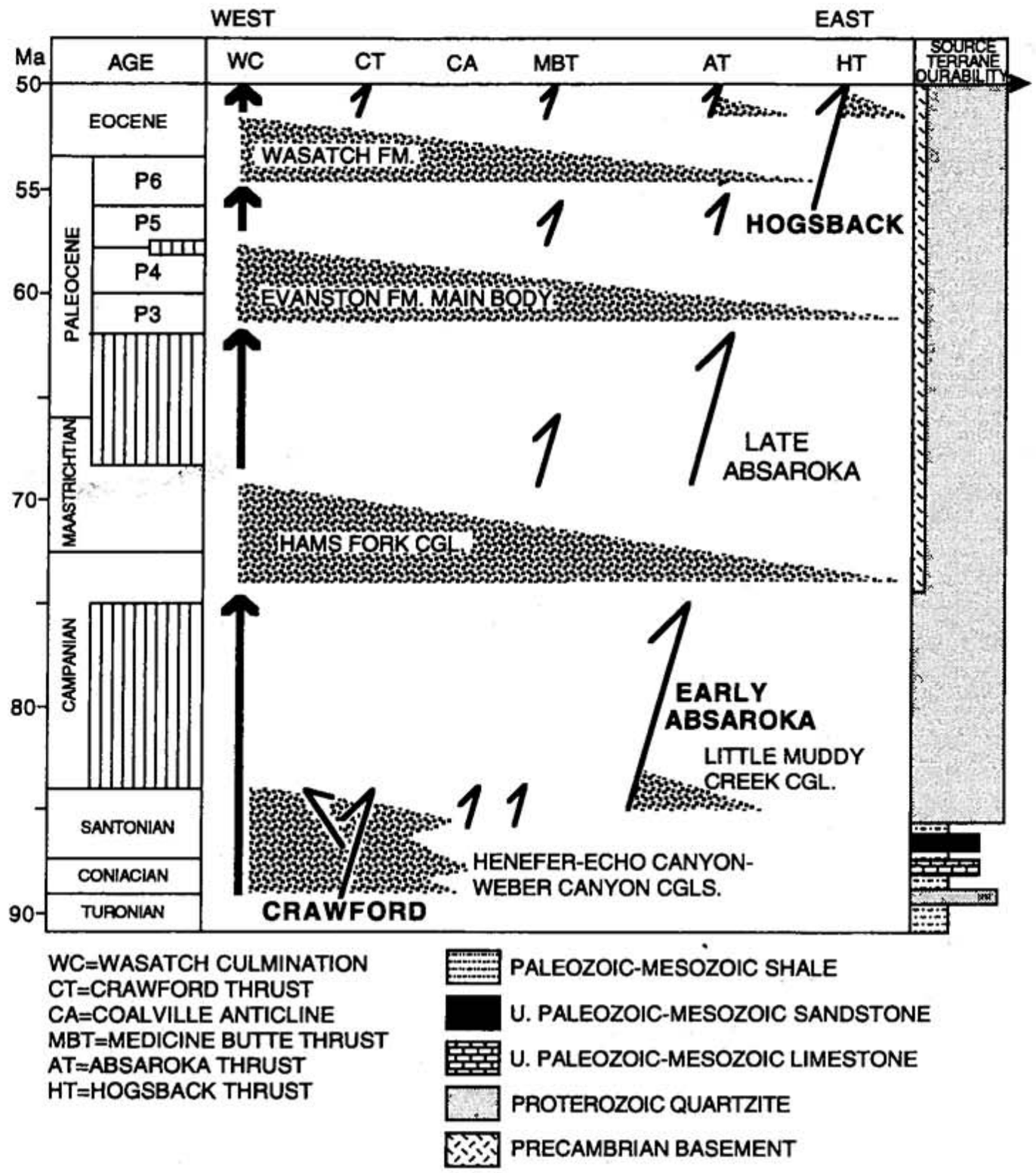

Figure 4. Simplified diagram showing the time-space history of thrust faulting, major erosional unconformities, and distribution of synorogenic sediments in the Sevier orogenic wedge in northeast Utah and southwest Wyoming (after DeCelles, 1994). Wedge-shaped stippled units of synorogenic sediment are not meant to imply volume or thickness. Generally, these units prograded eastward. Column at right illustrates the general composition of the synorogenic erosional surface in terms of relative durability (increasing toward the right) and rock types, with legend of rock types shown below.

DeCelles & Mitra, GSA Bull, 1995

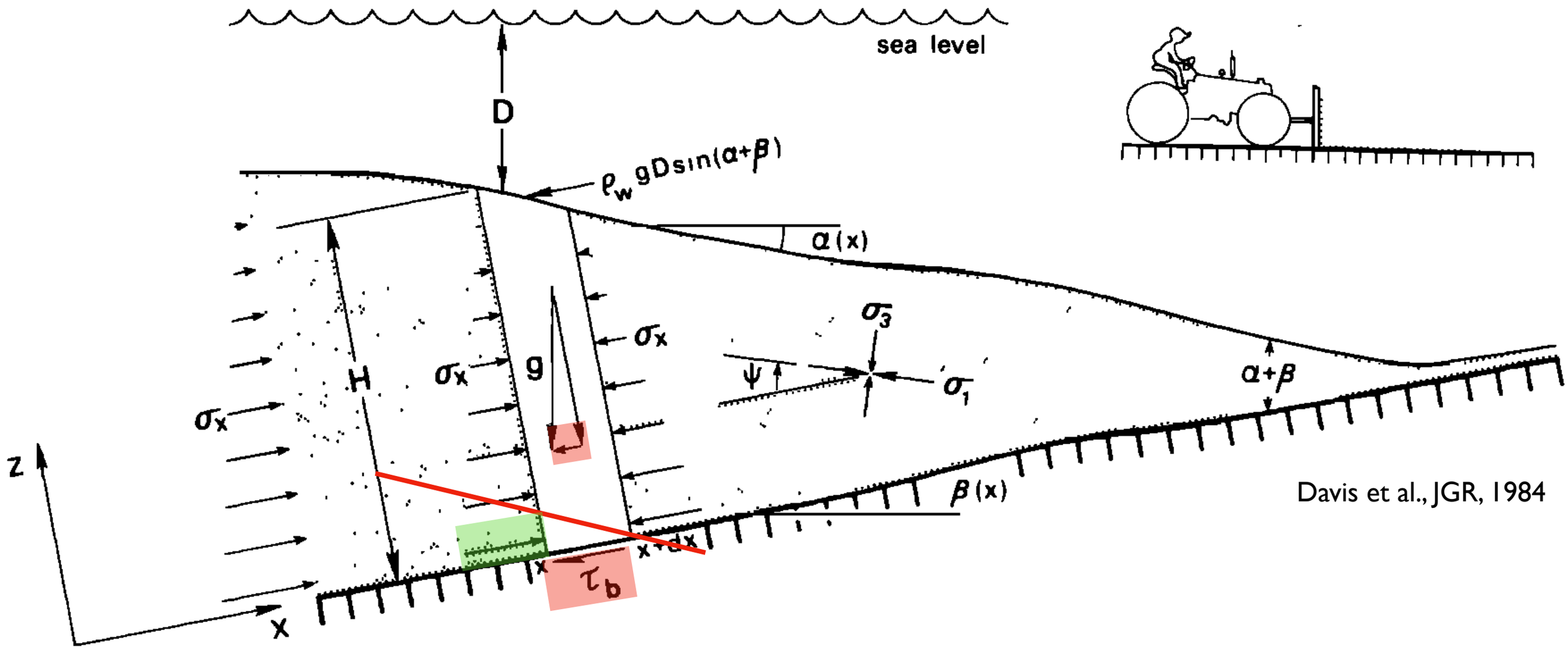

Davis et al., JGR, 1984

What happens if the geometry of the wedge changes?

If wedge thickens ($\alpha+\beta$ increase)

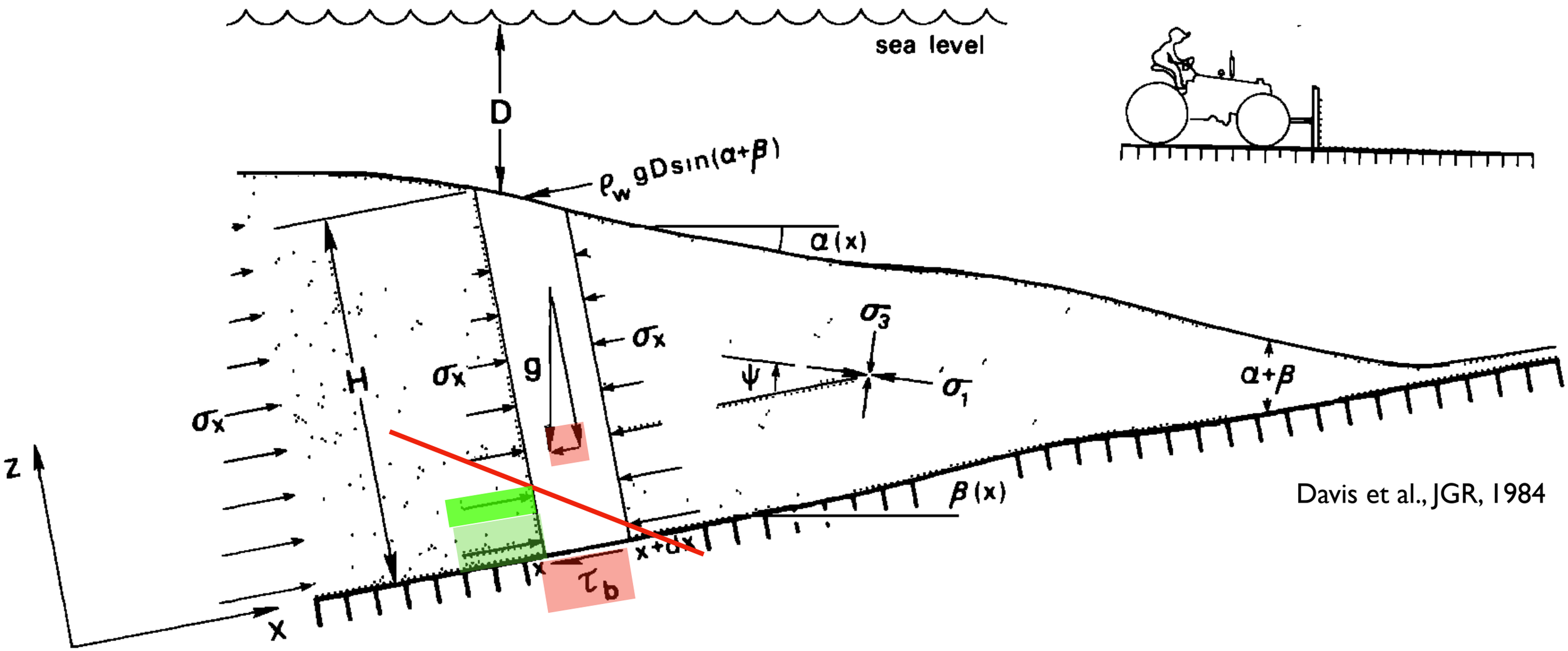

Davis et al., JGR, 1984

What happens if the geometry of the wedge changes?

If wedge thickens (α+β increase)

Extra force overcomes resistance and internal stresses relax as wedge moves forward on basal detachment

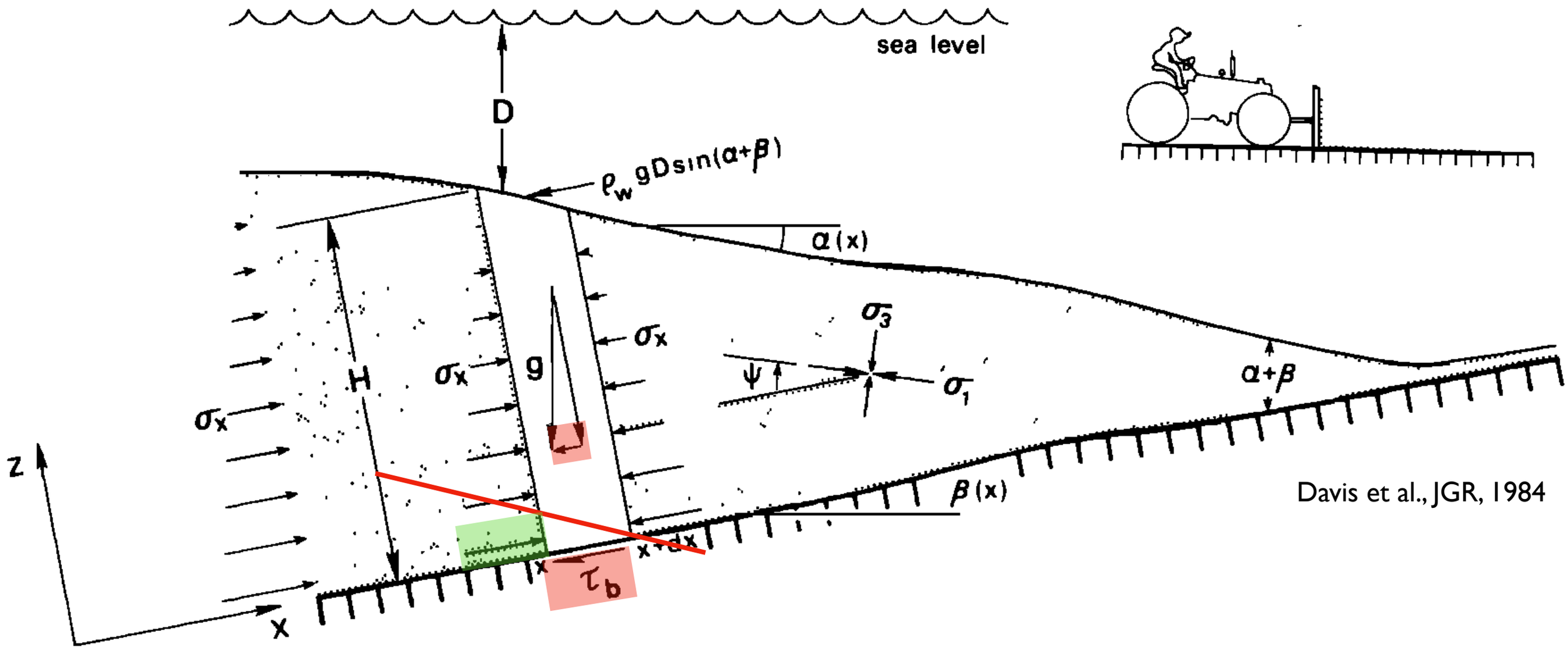

Davis et al., JGR, 1984

What happens if the geometry of the wedge changes?

If wedge thins ($\alpha+\beta$ decrease)

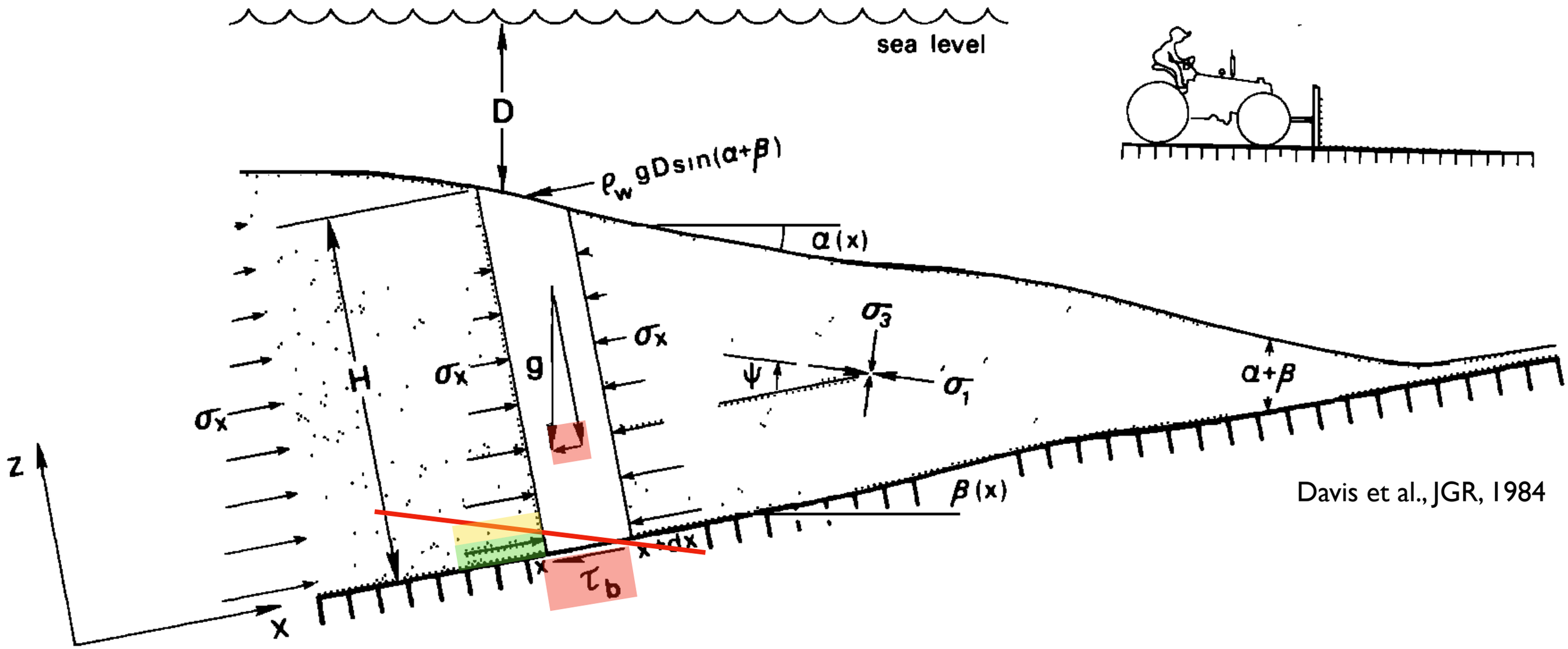

Davis et al., JGR, 1984

What happens if the geometry of the wedge changes?

If wedge thins ($\alpha+\beta$ decrease)

Insufficient force to overcome resistance; wedge stalls and has to thicken again to gain stress enough to move

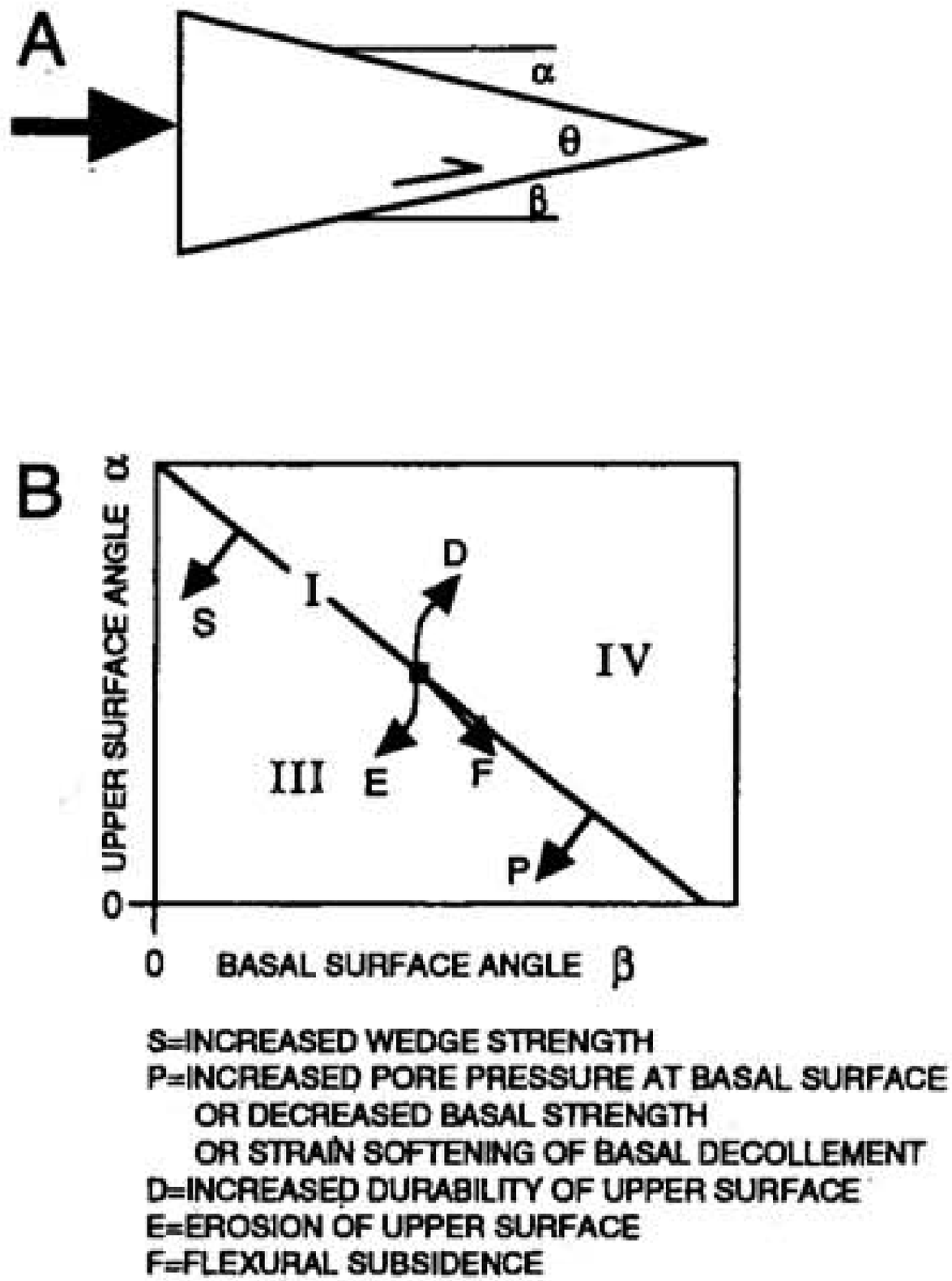

Figure 3. (A) Schematic diagram illustrating the geometry of a Coulomb wedge under the influence of a push from behind (arrow). Wedge taper (θ) equals the sum of surface slope (α) plus the angle of basal décollement (β). (B) Behavior of a Coulomb wedge in α-β space in response to changes in some key parameters (based on Davis et al., 1983; Dahlen, 1984; and Woodward, 1987). Labeled regions are as follows: I—critical, wedge advances in self-similar form by accretion of material across its base; III—subcritical, wedge is stalled because of insufficient taper; IV—supercritical, wedge is stable and capable of sliding forward along a single basal thrust. Changes E, D, and F affect a hypothetical wedge (denoted by the solid square) that initially has a critical taper. Changes S and P affect the location of the critical-taper line in α-β space.

DeCelles & Mitra,
GSA Bull, 1995

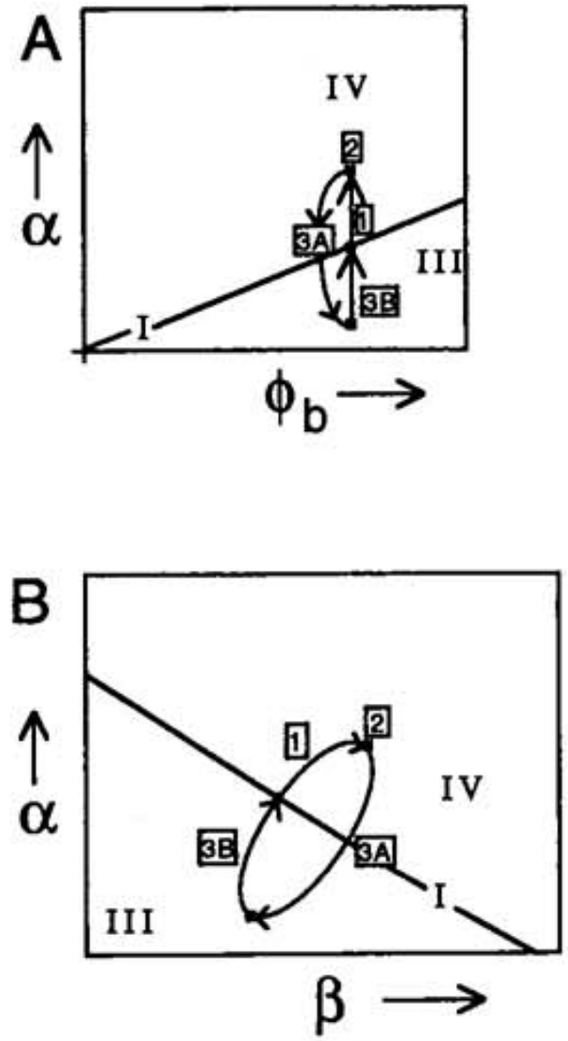

Figure 7. Schematic diagrams showing inferred short-term cycle of Sevier orogenic wedge behavior. Numbers in boxes refer to stages of the three-part cycle of Figure 5. (A) Wedge behavior in terms of upper-surface slope (α) and basal strength (ϕ_b). The wedge alternated between subcritical (III) and supercritical (IV) states during any given cycle, with no major change in basal strength. (B) Cyclic behavior of the wedge in terms of upper-surface slope and basal slope (β). Wedge alternated between regions III and IV, with probable minor changes in α and β. Changes illustrated in these diagrams would have been superimposed on the long-term behavior of the wedge shown in Figure 6.

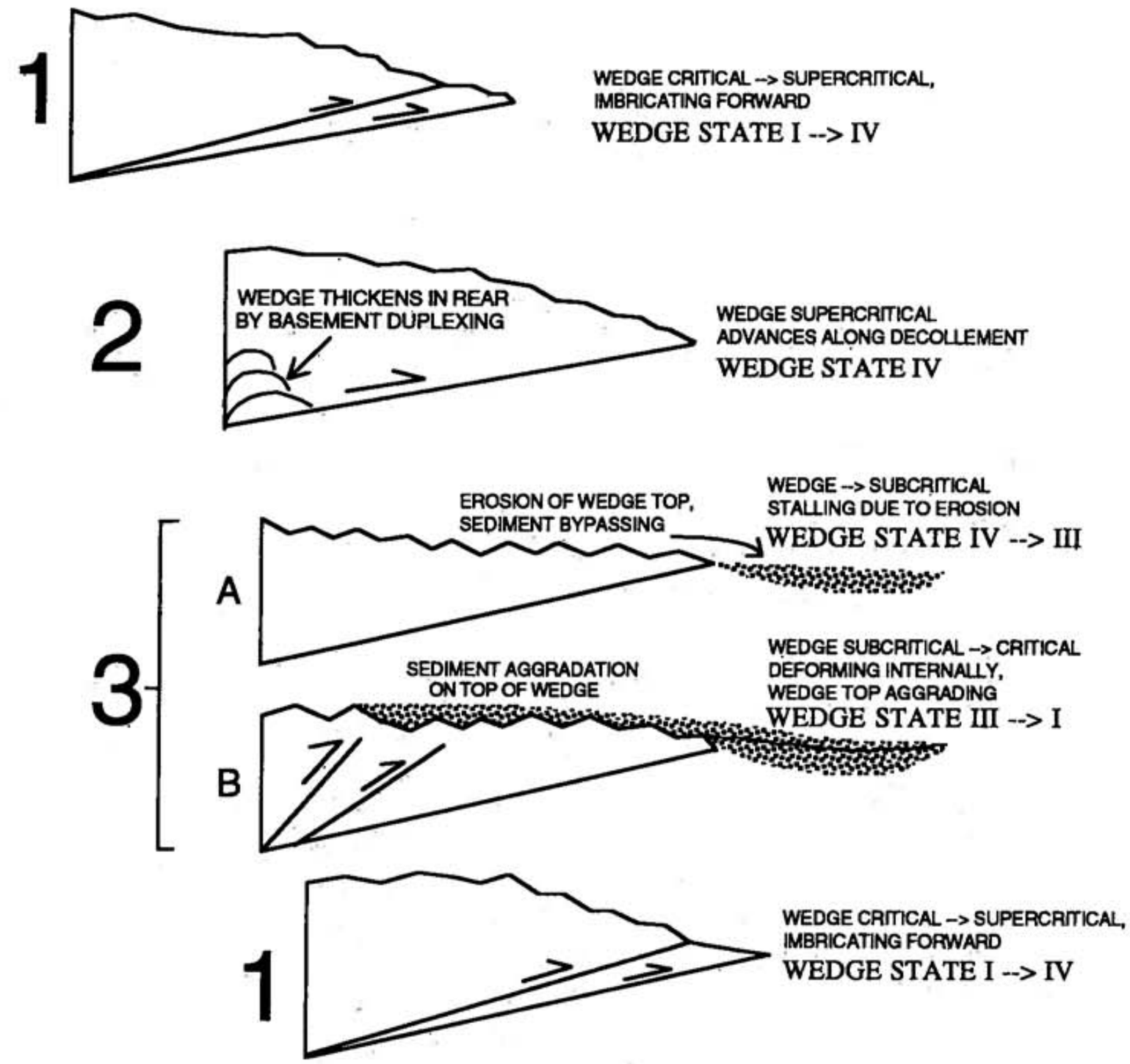

Figure 5. Schematic diagram illustrating the three-part cycle of Sevier orogenic wedge behavior in terms of inferred wedge taper. See text for discussion and Figure 3 for explanation of wedge states I, III, and IV.

DeCelles & Mitra, GSA Bull, 1995

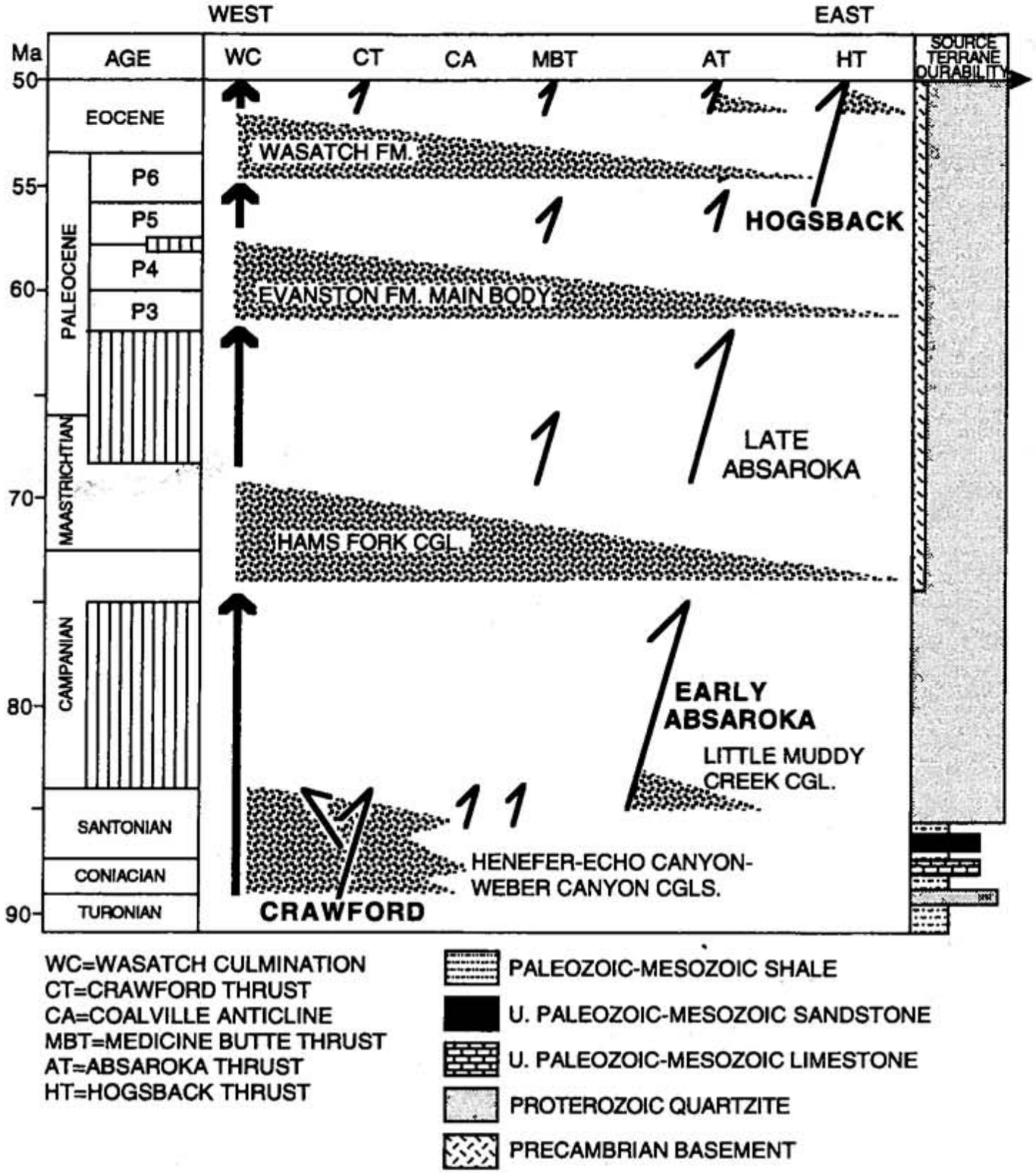

Figure 4. Simplified diagram showing the time-space history of thrust faulting, major erosional unconformities, and distribution of synorogenic sediments in the Sevier orogenic wedge in northeast Utah and southwest Wyoming (after DeCelles, 1994). Wedge-shaped stippled units of synorogenic sediment are not meant to imply volume or thickness. Generally, these units prograded eastward. Column at right illustrates the general composition of the synorogenic erosional surface in terms of relative durability (increasing toward the right) and rock types, with legend of rock types shown below.

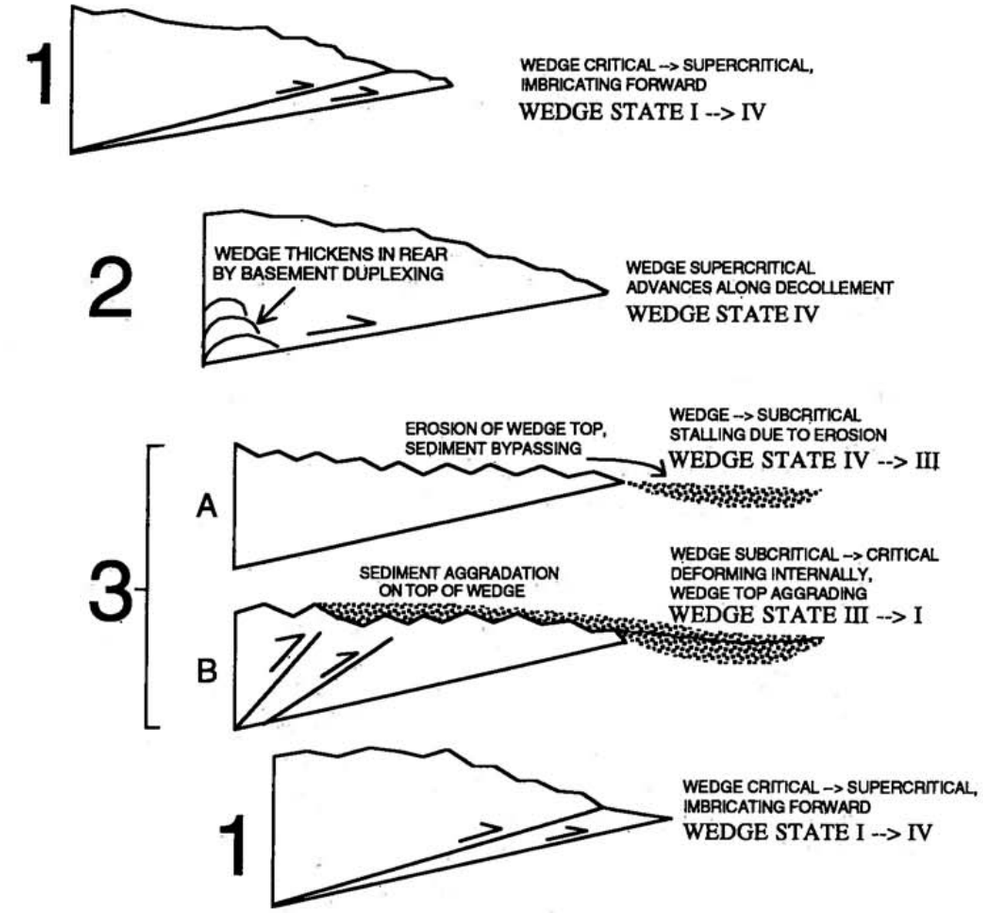

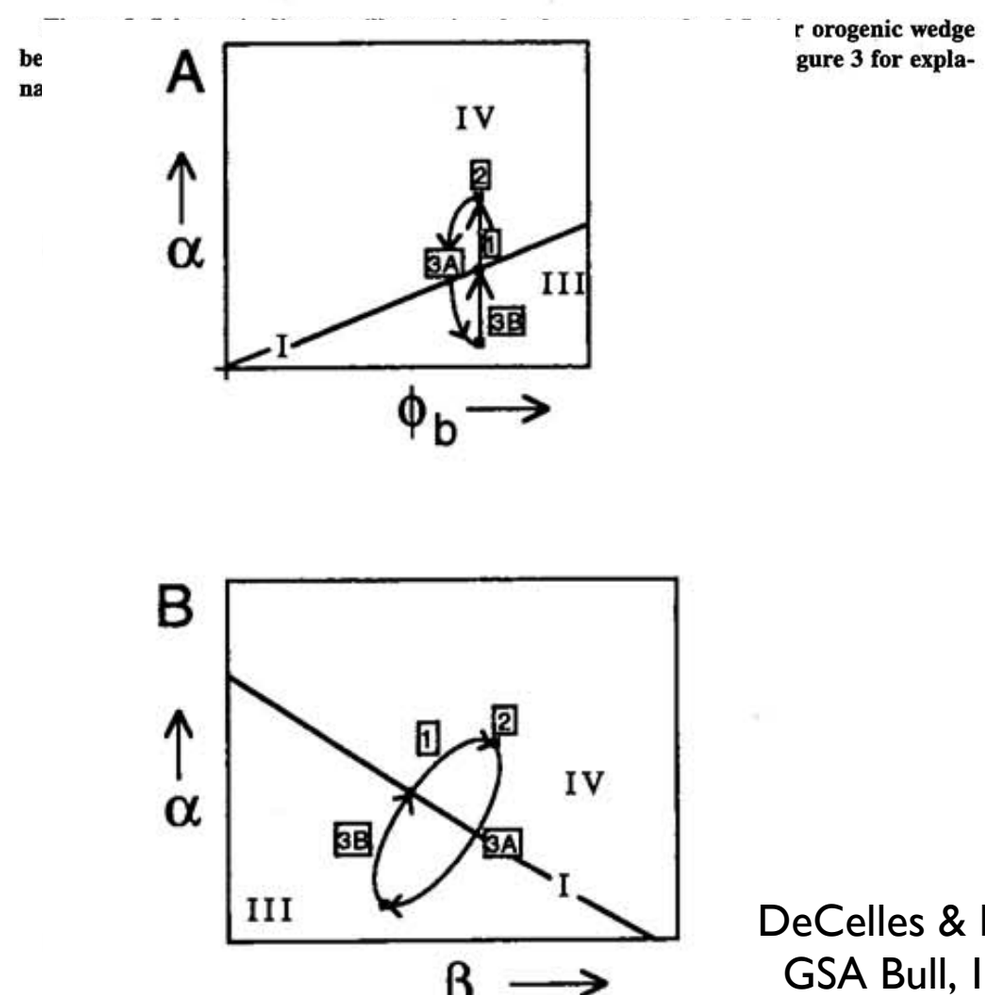

DeCelles & Mitra, GSA Bull, 1995